

# Splicing factor YBX1 mediates persistence of *JAK2*-mutated neoplasms

<https://doi.org/10.1038/s41586-020-2968-3>

Received: 11 December 2018

Accepted: 15 September 2020

Published online: 25 November 2020

 Check for updates

Ashok Kumar Jayavelu<sup>1,2,6</sup>, Tina M. Schnöder<sup>2,3,26</sup>, Florian Perner<sup>2</sup>, Carolin Herzog<sup>4</sup>, Arno Meiler<sup>1</sup>, Gurumoorthy Krishnamoorthy<sup>1</sup>, Nicolas Huber<sup>2</sup>, Juliane Mohr<sup>2</sup>, Bärbel Edelmann-Stephan<sup>4</sup>, Rebecca Austin<sup>5,6,7</sup>, Sabine Brandt<sup>8</sup>, Francesca Palandri<sup>9</sup>, Nicolas Schröder<sup>10</sup>, Berend Isermann<sup>11</sup>, Frank Edlich<sup>12,13,14</sup>, Amit U. Sinha<sup>15</sup>, Martin Ungelenk<sup>16</sup>, Christian A. Hübner<sup>16</sup>, Robert Zeiser<sup>13,17</sup>, Susann Rahmig<sup>18,19</sup>, Claudia Waskow<sup>18,19,20</sup>, Iain Coldham<sup>21</sup>, Thomas Ernst<sup>2</sup>, Andreas Hochhaus<sup>2</sup>, Stefanie Jilg<sup>22</sup>, Philipp J. Jost<sup>22,23</sup>, Ann Mullally<sup>24</sup>, Lars Bullinger<sup>25</sup>, Peter R. Mertens<sup>9</sup>, Steven W. Lane<sup>5,6,7</sup>, Matthias Mann<sup>1,27</sup> & Florian H. Heidel<sup>2,3,18,27</sup>✉

Janus kinases (JAKs) mediate responses to cytokines, hormones and growth factors in haematopoietic cells<sup>1,2</sup>. The *JAK* gene *JAK2* is frequently mutated in the ageing haematopoietic system<sup>3,4</sup> and in haematopoietic cancers<sup>5</sup>. *JAK2* mutations constitutively activate downstream signalling and are drivers of myeloproliferative neoplasm (MPN). In clinical use, JAK inhibitors have mixed effects on the overall disease burden of *JAK2*-mutated clones<sup>6,7</sup>, prompting us to investigate the mechanism underlying disease persistence. Here, by in-depth phosphoproteome profiling, we identify proteins involved in mRNA processing as targets of mutant JAK2. We found that inactivation of *YBX1*, a post-translationally modified target of JAK2, sensitizes cells that persist despite treatment with JAK inhibitors to apoptosis and results in RNA mis-splicing, enrichment for retained introns and disruption of the transcriptional control of extracellular signal-regulated kinase (ERK) signalling. In combination with pharmacological JAK inhibition, *YBX1* inactivation induces apoptosis in *JAK2*-dependent mouse and primary human cells, causing regression of the malignant clones in vivo, and inducing molecular remission. This identifies and validates a cell-intrinsic mechanism whereby differential protein phosphorylation causes splicing-dependent alterations of JAK2–ERK signalling and the maintenance of *JAK2*<sup>V617F</sup> malignant clones. Therapeutic targeting of *YBX1*-dependent ERK signalling in combination with JAK2 inhibition could thus eradicate cells harbouring mutations in *JAK2*.

*JAK2* is essential for the development of haematopoietic cells, and mutation of *JAK2* is a frequent event during ageing<sup>3,4</sup> that predisposes individuals to the development of haematologic cancers such as myeloproliferative neoplasms (MPN)<sup>5</sup>. Although treatment with JAK inhibitors reduces inflammatory activity and hyperproliferation of MPN, *JAK2*-mutated clones persist, undercutting the utility of this strategy<sup>6,7</sup>.

## Functional phosphoproteome profiling

To identify downstream effectors of the mutant *JAK2* kinase that may be responsible for this effect, we performed in-depth phosphoproteomics assays based on mass spectrometry (MS)<sup>8</sup> in mouse haematopoietic cells expressing the erythropoietin receptor and either wild-type *JAK2* (*JAK2*WT) or the mutant *JAK2*-V617F (*JAK2*VF; Fig. 1a). We exposed cells

<sup>1</sup>Max Planck Institute of Biochemistry, Munich, Germany. <sup>2</sup>Innere Medizin II, Hämatologie und Onkologie, Universitätsklinikum Jena, Jena, Germany. <sup>3</sup>Innere Medizin C, Universitätsmedizin Greifswald, Greifswald, Germany. <sup>4</sup>Department of Haematology and Oncology, Center of Internal Medicine, Otto von Guericke University Medical Center, Magdeburg, Germany. <sup>5</sup>QIMR Berghofer Medical Research Institute, Brisbane, Queensland, Australia. <sup>6</sup>Cancer Care Services, Royal Brisbane and Women's Hospital, Brisbane, Queensland, Australia. <sup>7</sup>University of Queensland, Brisbane, Queensland, Australia. <sup>8</sup>Department of Nephrology and Endocrinology, Center of Internal Medicine, Otto von Guericke University Medical Center, Magdeburg, Germany. <sup>9</sup>Azienda Ospedaliero–Universitaria di Bologna, Bologna, Italy. <sup>10</sup>Pathology, Klinikum Ernst-von-Bergmann, Potsdam, Germany. <sup>11</sup>Institute for Clinical Chemistry and Pathobiochemistry, Center of Internal Medicine, Otto von Guericke University Medical Center, Magdeburg, Germany. <sup>12</sup>Institute for Biochemistry and Molecular Biology, University of Freiburg, Freiburg, Germany. <sup>13</sup>Faculty of Biology, University of Freiburg, Freiburg, Germany. <sup>14</sup>BIOS, Centre for Biological Signaling Studies, Freiburg, Germany. <sup>15</sup>Basepair Technology Inc, New York, NY, USA. <sup>16</sup>Institut für Humangenetik, Universitätsklinikum Jena, Jena, Germany. <sup>17</sup>Department of Hematology and Oncology, Medical Center, Faculty of Medicine, University of Freiburg, Freiburg, Germany. <sup>18</sup>Leibniz Institute on Aging, Fritz Lipmann Institute, Jena, Germany. <sup>19</sup>Immunology of Aging, Leibniz Institute on Aging, Fritz Lipmann Institute, Jena, Germany. <sup>20</sup>Faculty of Biological Sciences, Friedrich Schiller University Jena, Jena, Germany. <sup>21</sup>Department of Chemistry, University of Sheffield, Sheffield, UK. <sup>22</sup>Medical Department III for Haematology and Oncology, Klinikum rechts der Isar, Technische Universität München, Munich, Germany. <sup>23</sup>Division of Oncology, Department of Internal Medicine, Medical University of Graz (MUG), Graz, Austria. <sup>24</sup>Division of Hematology, Department of Medicine, Brigham and Women's Hospital and Harvard Medical School, Boston, MA, USA. <sup>25</sup>Clinic for Hematology, Oncology and Tumor Immunology, Charité University, Berlin, Germany. <sup>26</sup>These authors contributed equally: Ashok Kumar Jayavelu, Tina M. Schnöder. <sup>27</sup>These authors jointly supervised this work: Matthias Mann, Florian H. Heidel. ✉e-mail: mmann@biochem.mpg.de; florian.heidel@uni-greifswald.de

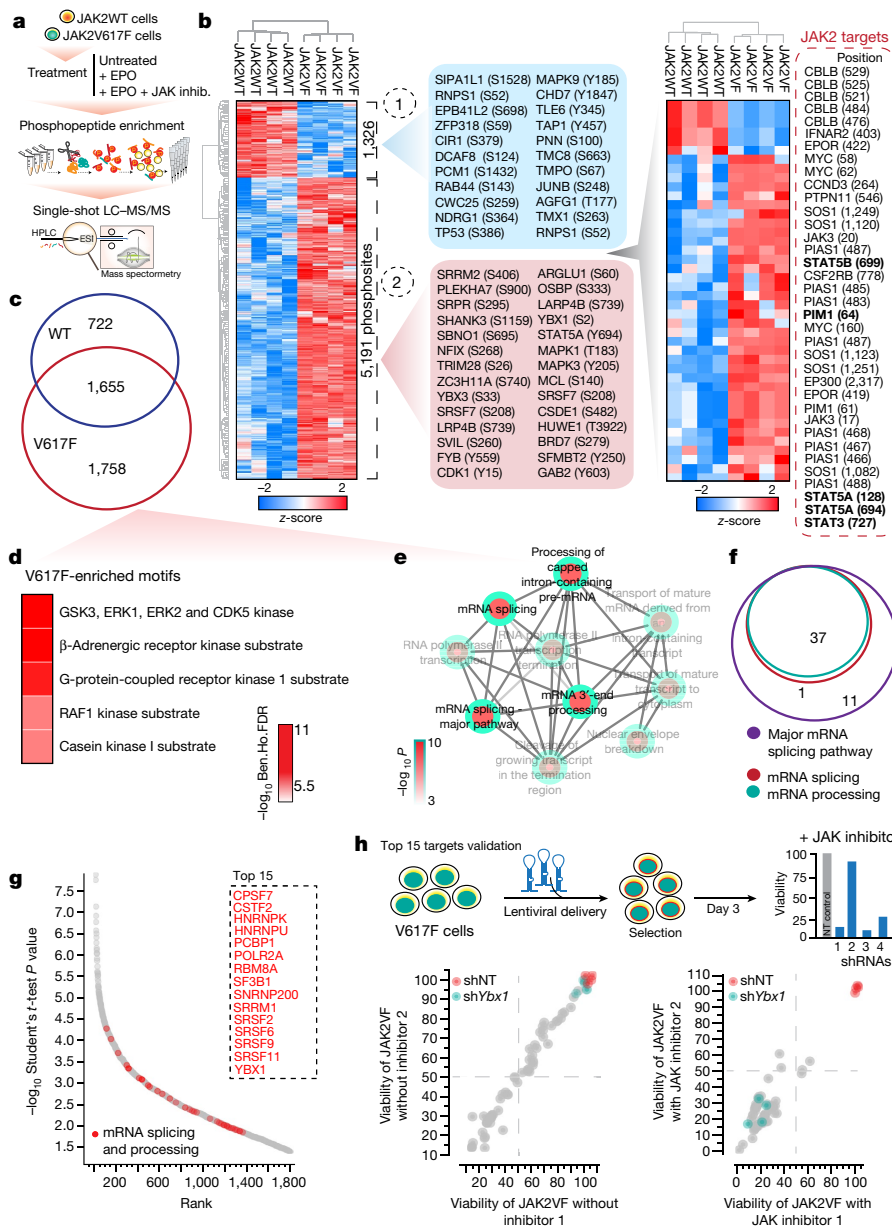


**Fig. 1 | Functional phosphoproteomics screen identifies the mRNA splicing and processing factor YBX1 downstream of JAK2V617F.** **a**, Experimental setup of the screen. **b**, Unsupervised hierarchical clustering of significantly ( $t$ -test with permutation-based FDR  $< 0.01$ ) regulated phosphosites in JAK2WT and JAK2VF cells. Panel highlight shows top upregulated phosphoproteins in JAK2WT (cluster 1) and JAK2VF (cluster 2) cells, along with amino acid positions of the individual phosphosites, of significantly regulated JAK2-STAT signalling pathway members. Heatmap at right shows enrichment of known JAK2-STAT signalling targets in JAK2WT and JAK2VF cells. **c**, Venn diagram showing proteins differentially phosphorylated in JAK2WT cells, JAK2VF cells and both. **d**, Heatmap representation of motifs significantly enriched in JAK2VF cells assessed by Fisher's exact test (Benjamin-Hochberg FDR value ( $-\log_{10}$  Ben.

Ho. FDR) shown). **e**, Sub-network map of significantly enriched ( $P < 0.01$ ) GO terms of proteins differentially phosphorylated in JAK2VF. Colours of nodes range from bright to transparency based on  $P$  value. Highlighting indicates core components of the sub-network. Two-sided hypergeometric test,  $P$  value correction-Bonferroni stepdown (also Extended Data Fig. 2a). **f**, Venn diagram showing number of proteins common to nodes highlighted in e. **g**, Ranking of proteins significantly phosphorylated in JAK2VF. Those participating in mRNA splicing and processing are highlighted in red, with the top 15 listed at right (in alphabetical order). **h**, shRNA validation of selected top 15 targets essential for JAK2VF cell survival and growth in the presence and absence of JAK inhibitor (ruxolitinib, 0.5  $\mu$ M) measured by MTS colorimetric assay (four biologically independent experiments with eight technical replicates each).

to erythropoietin alone or combined with a JAK inhibitor (ruxolitinib) to investigate erythropoietin-independent and JAK-inhibitor-responsive signalling in JAK2VF as compared to JAK2WT cells. We quantified 21,764 distinct, localized phosphorylated sites on 4,135 different proteins (Extended Data Fig. 1a-e). Of 6,517 phosphosites identified as regulated in JAK2VF and JAK2WT at a false discovery rate (FDR) of 5%, we found 5,191 distinctly regulated in JAK2VF cells on 1,758 proteins, including previously known targets of JAK2, such as STAT5, STAT3 and PIM (Fig. 1b,c). Kinase motifs for glycogen synthase kinase-3 (GSK3), ERK

and cyclin-dependent kinases (CDKs) were also enriched among these phosphosites (Fig. 1d). Notably, gene ontology analysis indicated that the cellular processes most highly enriched in JAK2VF versus JAK2WT cells were mRNA splicing and processing (Fig. 1e and Extended Data Fig. 1f). To assess the potential functional roles of members of the mRNA splicing and processing pathways (Fig. 1f), we chose the 15 top-ranked proteins (based on  $P$  values) of a total of 47 pathway members for an RNA interference (RNAi) screening (Fig. 1g). We used four or five shRNAs per gene, confirmed knockdown efficiencies and assessed the growth

of the cells carrying the knockdowns with and without JAK inhibitor (70 shRNAs against 15 candidates and 4 non-targeting controls; Extended Data Figs. 1g–i and 2a). Targeting HNRNP, SRSF2 and SRSF9 resulted in dropouts, with at least three of the four shRNAs resulting in significant growth impairment. Other targets appeared dispensable for the proliferation and survival of JAK2VF cells, but their inactivation sensitized persistent cells to JAK inhibition (Fig. 1h). Given the persistence of JAK2VF clones after JAK inhibitor therapy in patients with MPN, we reasoned that these proteins might offer strategies to target disease persistence in vivo. The most prominent candidate, and the only one showing positive results with four of four shRNAs and exclusively in the presence of JAK inhibitor (Extended Data Fig. 2a), was the pleiotropic Y-box-binding protein 1 (YBX1). YBX1 sensitized JAK2VF cells to treatment with JAK inhibitor and is a core spliceosomal protein<sup>9</sup> that regulates mRNA splicing in various cellular contexts<sup>10–13</sup> (Fig. 1h).

### Dependency of JAK2VF cells on YBX1

We found that YBX1 was highly expressed in 76 primary bone marrow biopsies of patients diagnosed with JAK2-mutated MPN (Fig. 2a, b) compared to normal bone marrow ( $n = 18$ ). Moreover, YBX1 colocalized with and bound to JAK2 in JAK2VF cells (Extended Data Fig. 2b, c). Genetic inactivation of YBX1 in the mouse JAK2VF cells resulted in reduced proliferation in vitro when the cells were exposed to JAK inhibitor, with a decline in  $IC_{50}$  from 1,000 nM to 275 nM (Fig. 2c). YBX1 depletion alone did not affect viability, proliferation, cell cycle activity, ROS production or DNA damage in either JAK2WT or JAK2VF cells (Extended Data Fig. 2d–i). Instead, the reduction in the growth of JAK2VF cells lacking YBX1 when exposed to JAK inhibitor seemed to be due to the induction of apoptosis (Fig. 2d–f). We confirmed these findings in JAK2VF-mutated mouse (Fig. 2d) and human (Fig. 2e) cell lines, as well as primary lineage-depleted *Jak2*<sup>VF</sup> (*Jak2*<sup>VF</sup>) mouse bone marrow cells (Fig. 2f and Extended Data Fig. 2j).

To assess YBX1 as a potential therapeutic target in JAK2-mutated neoplasms, we tested whether genetic inactivation would reduce the proportion of clones that persist under JAK inhibitor treatment. We generated a conditional knockout mouse model with exon 3 of *Ybx1* flanked by loxP sites (*Ybx1*<sup>fl/fl</sup>; Extended Data Fig. 3a, b) and crossed this with conditional *Jak2*<sup>VF</sup> knock-in mice harbouring an inducible Mx1-Cre recombinase. Bone marrow from *Ybx1*<sup>fl/fl</sup> *Jak2*<sup>VF</sup> Mx1<sup>+</sup> and *Ybx1*<sup>+/+</sup> *Jak2*<sup>VF</sup> Mx1<sup>+</sup> or *Ybx1*<sup>fl/fl</sup> *Jak2*<sup>VF</sup> Mx1<sup>+</sup> littermate controls (all CD45.2) was transplanted in a competitive manner along with competitor cells. After engraftment of transplanted cells, recipient animals received injections of polyinosinic–polycytidylic acid (pIpC) to activate Mx1-Cre and genetically delete *Ybx1*, along with JAK inhibitor administered by gavage. Recipients of *Jak2*<sup>VF</sup> *Ybx1*<sup>+/+</sup> bone marrow showed hyperleukocytosis, thrombocytosis and the onset of symptomatic splenomegaly. In contrast, *Ybx1*-deficient *Jak2*<sup>VF</sup> clones did not induce symptomatic disease within 16 weeks after transplantation (Fig. 2g–i). Testing for peripheral blood chimerism revealed an increasing percentage of CD45.2 JAK2VF cells, whereas genetic inactivation of YBX1 resulted in suppression or loss of the *Jak2*-mutated clone when the cells were also treated with JAK inhibitor (Fig. 2j, Extended Data Fig. 3c). After 20 weeks, 5 of 9 recipients had lost *Jak2*<sup>VF</sup> cells (<1% CD45.2 cells in peripheral blood and bone marrow), whereas all controls showed notably increased peripheral blood chimerism (Fig. 2k). Four of nine recipients of *Ybx1*<sup>fl/fl</sup> *Jak2*<sup>VF</sup> Mx1<sup>+</sup> bone marrow showed counter-selection of clones with incomplete excision of *Ybx1*, indicative of selective pressure. Consistent with this, development of myeloid hyperplasia in the bone marrow and organ infiltration (Extended Data Fig. 3d, e) was blunted in recipients of YBX1-depleted cells. In a xenograft model of JAK2VF-mutated human cells, RNAi-mediated inactivation of YBX1 followed by saline injection did not significantly delay disease progression (Fig. 2l), but inactivation of YBX1 with concurrent JAK inhibitor treatment significantly prolonged survival and led to loss of disease

penetrance in 4 of 12 recipients (Fig. 2m). Notably, JAK inhibition alone delayed disease progression only slightly (NT + diluent, OS 27 vs 30 d; NT + JAK inhibition, OS 27 vs 72 d). We conclude that the persistence of *Jak2*-mutated clones under pharmacologic JAK inhibition can be disrupted in human and mouse cells by eliminating YBX1.

To be clinically relevant, such treatment must have a suitable therapeutic index between haematopoietic stem and progenitor cells (HSPCs) and their malignant counterparts, particularly given the role of YBX1 in mRNA processing and splicing. Of note, genetic inactivation of *Ybx1* did not perturb steady-state haematopoiesis (Extended Data Fig. 3f–j), and YBX1-deficient (lineage ‘Sca-1’<sup>Kit</sup><sup>+</sup>, LSK) HSPCs did not reveal any significant disadvantage in colony-forming potential or lineage commitment compared to *Ybx1*<sup>+/+</sup> controls (Extended Data Fig. 3k–n). Furthermore, functional impairment of adult YBX1-deficient mouse long-term haematopoietic stem cells was excluded by serial transplantation into primary (Fig. 2n, Extended Data Fig. 3o) and secondary recipient hosts (Fig. 2o, Extended Data Fig. 3p). Thus, inactivation of *Ybx1* does not impair the function of HSPCs in vitro or in vivo.

### YBX1 is required for MKNK1 splicing

To gain further insight into the regulation of YBX1 by mutant JAK2, we investigated the phosphoprofile of YBX1 in JAK2VF cells. In cells treated with erythropoietin and JAK inhibitor, YBX1 was specifically phosphorylated at several phosphosites in JAK2VF as compared to JAK2WT cells (Extended Data Fig. 4a–c). To further characterize post-translational modulators of YBX1, we performed phosphoproteome analysis following pharmacologic short-term inhibition of several bona fide downstream effectors of JAK2 (Extended Data Fig. 4d, e). This identified significant changes in the phosphorylation of the pS30 and pS34 residues of YBX1 that occurred only upon treatment with a MEK and ERK inhibitor (PD0325901) and were conserved across species (Extended Data Fig. 4f, g). To corroborate the YBX1–MAPK interaction, we performed YBX1 affinity purification combined with quantitative interaction proteomics, which revealed 260 JAK2VF-dependent interactors (Extended Data Fig. 5a). Among these, ribonucleoproteins, mRNA splicing factors and ribosomal proteins were significantly enriched (Extended Data Fig. 5b–e), which also explains the large number of interactors ( $P < 0.05$ ). Most notably, this analysis identified as YBX1 interactors in *Jak2*-mutated cells several bona fide members of mRNA splicing complexes that are known to interact during the formation and activation of spliceosomes (44/134 core splicing factors that participate in several steps of dynamic spliceosome assembly; Extended Data Fig. 5b–d). We also discovered that JAK2 and MAPK1 interact (Extended Data Fig. 5e, f) indicating that YBX1 may be recruited and regulated by the JAK2–MAPK1 axis. Furthermore, the interactome of VF cells treated with JAK inhibitor confirmed that the YBX1–MAPK1 interaction is independent of JAKs (Extended Data Fig. 5g, h). To delineate the relevance of this regulation of YBX1 phosphorylation sites induced by MEK inhibitor, we expressed YBX1 phosphomutants mimicking hyper- or hypophosphorylated states at conserved and relevant serine residues in *Jak2*-mutated cells (Extended Data Fig. 6a). Expression of pS30A, pS34A or pS30A pS34A (double) phosphomutants (but not pS30D, pS34D, pS30D pS34D or pS170A pS172A mutants) resulted in reduction of nuclear YBX1 translocation (Extended Data Fig. 6b, c). Moreover, these modifications recapitulated the phenotype of genetic inactivation and sensitized *Jak2*-mutated cells to cell death mediated by JAK inhibitor (Extended Data Fig. 6d–f). Consistent with this, treatment with MEK inhibitor alone or in combination with JAK inhibitor, but not with JAK inhibitor only, prevented nuclear import of YBX1 to a significant degree in mouse and human *Jak2*-mutated cells (Extended Data Fig. 7a–e). These data suggest that MAPK signalling stabilizes nuclear YBX1, a notion that was further supported by impaired binding of the YBX1 pS30A and pS34A phosphomutants to MAPK1 (Extended Data Fig. 7f). Collectively our data demonstrate that YBX1 undergoes

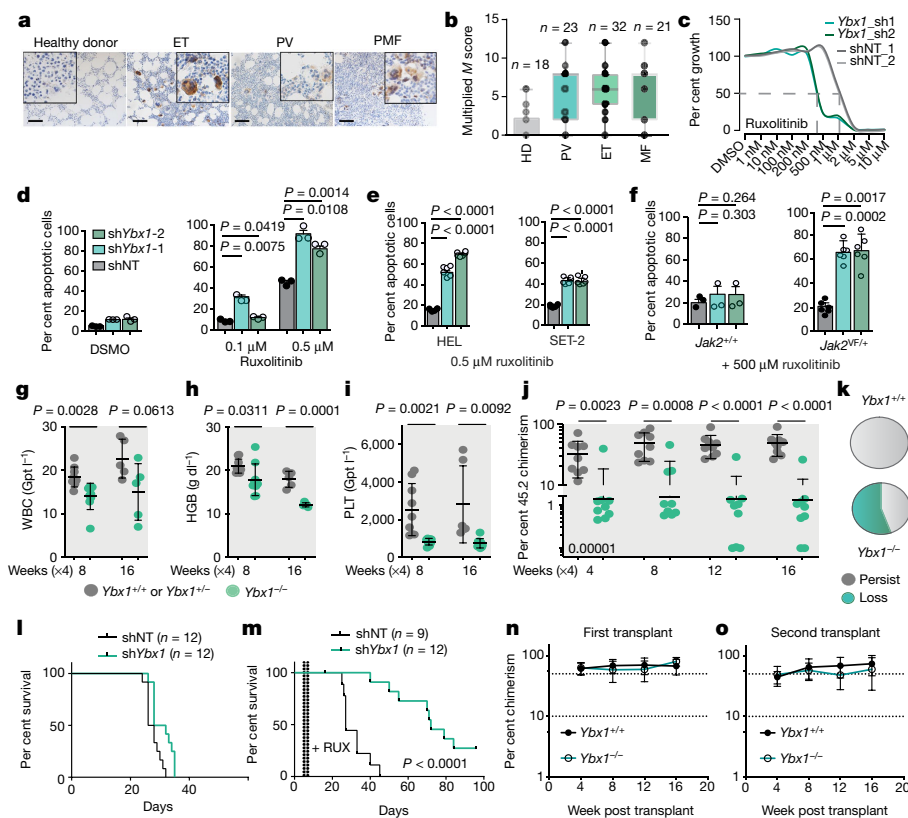


**Fig. 2 | Inactivation of *YBX1* selectively sensitizes *JAK2VF* cells to apoptosis induced by *JAK* inhibitor. **a**, Immunohistochemistry for *YBX1* in bone marrow biopsies of patients with MPN and healthy donor (HD) controls. Scale bars, 200  $\mu\text{m}$ . HD,  $n = 18$ ; MPN, essential thrombocythemia (ET)  $n = 32$ , polycythemia vera (PV)  $n = 23$ , myelofibrosis (MF)  $n = 21$ . **b**, Quantification of *YBX1* abundance in *JAK2VF*<sup>+</sup> bone marrow biopsies (multiplied *M* score). Box plots: mean  $\pm$  s.d., 10th–90th percentile. **c**, Cell growth of *JAK2VF* cells after lentiviral infection with shRNAs targeting *Ybx1* (*Ybx1*\_sh1 and *Ybx1*\_sh2) or non-targeting control shRNAs (shNT\_1 and shNT\_2) and treatment with *JAK* inhibitor (ruxolitinib; 1 nM–10  $\mu\text{M}$ ), measured by MTS assay ( $n = 4$ , 8 technical replicates). **d–f**, Percentages of apoptotic cells (mean  $\pm$  s.d.) upon *JAK* inhibitor treatment following knockdown of *Ybx1* (sh*Ybx1*-1/2 RNAi) versus control shRNA treatment (shNT RNAi) in mouse Ba/F3 *JAK2VF* cells (**d**;  $n = 3$ ), the human *JAK2VF*<sup>+</sup> cell lines HEL and SET-2 (**e**;  $n = 5$  each) and lineage-negative primary mouse bone marrow cells (**f**; *Jak2*<sup>+/+</sup>,  $n = 3$ ; *Jak2*<sup>+/VF</sup>,  $n = 6$ ). **g–k**, Persistence of *JAK2VF*<sup>+</sup> clones after treatment with *JAK* inhibitor following genetic inactivation of *Ybx1*. Treatments were with *JAK* inhibitor (90 mg  $\text{kg}^{-1}$ , twice a**

day, by oral gavage) or low-molecular-weight pIpC (5 mg  $\text{kg}^{-1}$  daily intraperitoneally) on days 10–15 after engraftment of donor cells. **g–i**, Peripheral blood counts of recipient mice, weeks 8 and 16: white blood cells (WBC; **g**), haemoglobin (HGB; **h**) and platelets (PLT; **i**) of *Jak2*<sup>+/VF</sup> *Ybx1*<sup>-/-</sup> and *Jak2*<sup>+/VF</sup> *Ybx1*<sup>+/+</sup> mice ( $n \geq 5$  each; mean  $\pm$  s.d.). **j**, Peripheral blood chimerism of irradiated (12 Gy) recipient mice. Percentages of *Jak2*<sup>+/VF</sup> *Ybx1*<sup>+/+</sup> or *Jak2*<sup>+/VF</sup> *Ybx1*<sup>-/-</sup> (CD45.2) cells and CD45.1 competitors, weeks 4–16 ( $n = 9$ ; mean  $\pm$  s.d.). **d–j**, *P* values determined by two-tailed *t*-test. **k**, Percentages of mice with loss (green) or persistence (grey) of *Jak2*<sup>+/VF</sup> clones in *Ybx1* WT and knockout recipients. **l, m**, Kaplan–Meier survival curves of irradiated (2 Gy) recipient NSGS mice transplanted with HEL cells expressing sh*Ybx1*-1/2 or shNT without (**l**;  $n = 12$  each) or with (**m**;  $n = 12$ , 9, respectively) subsequent *JAK* inhibitor treatment (RUX; 90 mg  $\text{kg}^{-1}$  twice a day, by gavage, days 5–10). Log-rank test. **n, o**, Peripheral blood chimerism of CD45.2 *Ybx1*<sup>+/+</sup> or *Ybx1*<sup>-/-</sup> ( $n = 9$  each) cells compared to CD45.1/2 cells (competitors) of primary (**n**) and secondary (**o**) recipient mice, weeks 4–16. Two independent cohorts; mean  $\pm$  s.d. **a–o**,  $n$  indicates independent biological replicates.

phosphorylation dependent on *JAK2VF* and *MAPK1* and that the interaction of *YBX1* and *MAPK1* is crucial for nuclear translocation of *YBX1* and persists despite treatment with *JAK* inhibitor.

To identify the transcriptional pathways controlled by *YBX1*, we performed RNA sequencing (RNA-seq) analysis of mouse and human *Jak2*-mutated cells after inactivation of *YBX1* by RNAi. Gene ontology (GO) analysis of the differentially expressed coding genes revealed strong signatures of inflammation, chemotaxis and cytokine production but also of *MAPK* and *ERK* signalling and programmed cell death (Fig. 3a, b). Given the established role of *YBX1* in mRNA splicing, we analysed altered splicing by transcriptome profiling of mouse *Jak2*-mutated cells and detected a 70% increase in intron retention (1,064 events,  $P < 0.05$  and  $\Delta\text{PSI} > 0.1$ ) compared to that in controls (Fig. 3c, Extended Data Fig. 8a, b). GO term analysis of genes with elevated intron retention in cells with *YBX1* activation revealed that these were enriched for terms related to RNA splicing, nonsense-mediated decay, apoptosis and *MAPK* signalling (472 events,  $P < 0.01$ ,  $\Delta\text{PSI} > 0.1$ ; Extended Data Fig. 8c). Depending on localization, intron retention can result

in initiation of translation, nuclear degradation, nonsense-mediated mRNA decay (NMD) or mRNA stabilization. We then asked whether *ERK* signalling molecules encoded by genes showing increased intron retention, such as *Araf*, *Braf* and *Mknk1*, were regulated in *Jak2*-mutated cells (Fig. 3d). Comparing the global mRNA and protein abundance of *ERK* signalling proteins showed significant decreases for *BRAF* (mRNA) and *MKNK1* (mRNA and protein) (Fig. 3e). Western blotting confirmed the loss of *MKNK1* expression in *YBX1*-depleted *JAK2VF* mouse and human cells (Fig. 3f, g). Treatment with the mRNA splicing inhibitors herboxidiene and pladeinolide B, which target spliceosome machinery, confirmed that the expression of *MKNK1* is dependent on efficient splicing of *Mknk1* (Fig. 3h, i). In vitro splicing assays confirmed that *YBX1* is required for the splicing of *Mknk1* pre-mRNA in mouse *JAK2VF* cells (Extended Data Fig. 8d). Additionally, targeting the NMD pathway with dorsomorphin (compound c, termed CC) or *VG-1* inhibitor treatment resulted in dose-dependent rescue of *MKNK1* translation (Extended Data Fig. 8e, f). Of note, *YBX1* chromatin immunoprecipitation sequencing (ChIP-seq) revealed no significant binding to *Mknk1*



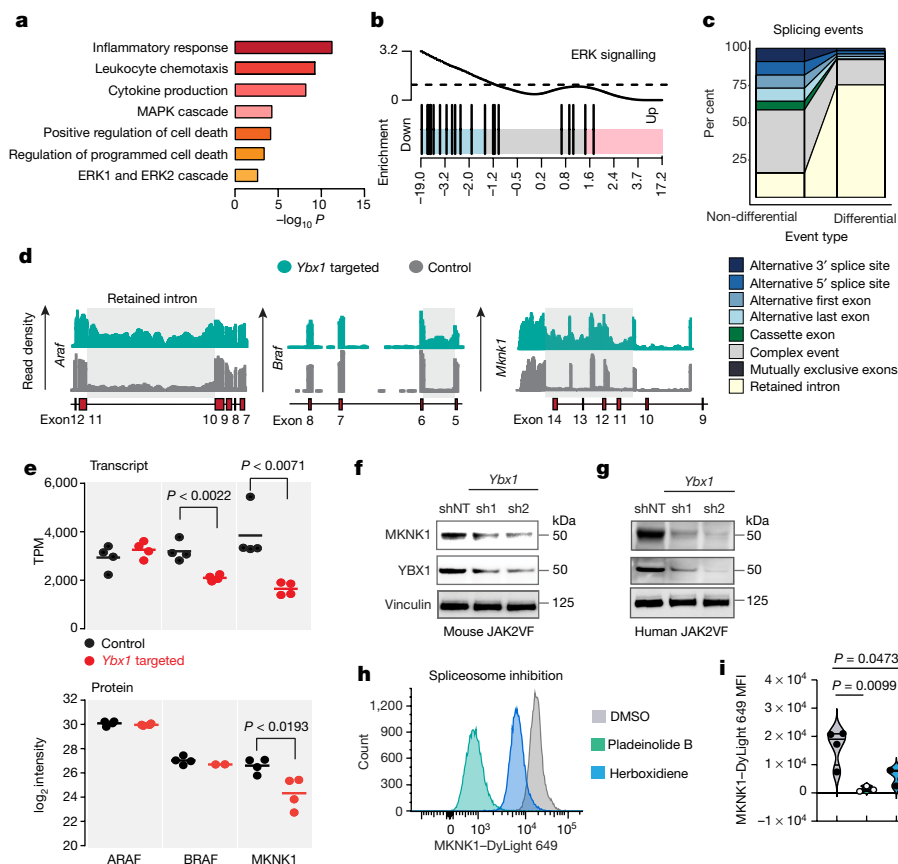


**Fig. 3 | Targeting YBX1 in JAK2VF cells promotes intron retention.** **a**, Gene ontology enrichment analysis of genes differentially expressed after inactivation of *Ybx1* in mouse JAK2VF cells. Bar plot shows significantly deregulated pathways, with Fisher's exact test *P* values on *x*-axis. **b**, Gene-set enrichment analysis (GSEA) depicting negative enrichment of genes related to ERK signalling after inactivation of YBX1. **c**, Percentages and types of splicing events (1,943 differential splicing events with two-tailed test *P* < 0.05) differentially regulated following inactivation of YBX1; 'retained intron' (yellow) is the significantly (70%) upregulated splicing event. **d**, Retained intron read density profile between indicated exon–intron locations of *Araf*, *Braf* and *Mknk1* in control (*n* = 4) and *Ybx1*-targeted cells (*n* = 4). **e**, Transcript

(transcripts per million, by RNA-seq) and protein ( $\log_2$  fold change, by proteome analysis) expression levels of ARAF, BRAF and MKNK1 in control and YBX1-depleted mouse JAK2VF cells (*n* = 4, two-tailed *t*-test). **f**, **g**, Representative western blot (of *n* = 3) validation of MKNK1 protein abundance after inactivation of YBX1 in mouse Ba/F3 JAK2VF and human HEL cells. **h**, Representative flow cytometry histograms showing MKNK1 levels of mouse JAK2VF cells after 8-h treatment with herboxidiene (25 nM) or pladeinolide B (10 nM). **i**, Violin plot showing MKNK1 abundance (indicated by mean fluorescence intensity (MFI)) after herboxidiene or pladeinolide B treatment (*n* = 4; two-tailed *t*-test). **f**–**i**, *n* indicates independent biological replicates.

genomic regions in either mouse or human JAK2VF cells (Extended Data Fig. 8g, h). Consistent with this, expression of YBX1 phosphomutants (S30A, S34A and S30A S34A) resulted in reduction or abrogation of MKNK1 production (Extended Data Fig. 8i), confirming that phosphorylation of YBX1 at Ser30 and Ser34 in JAK2VF cells is a critical requirement for efficient mRNA splicing and transcriptional regulation of *Mknk1* transcripts and a mechanistic link to the YBX1-dependent disruption of ERK signalling.

### Targeting of MKNK1–ERK signalling

Phosphoproteome profiling of YBX1-targeted mouse and human JAK2VF cells revealed significant downregulation of phosphosites, with key phosphorylation changes in substrates enriched for ERK1/2, GSK3 and CDK motifs (2,012 sites in mouse and 2,390 sites in human, FDR < 0.01; Fig. 4a, b and Extended Data Fig. 9a, b). Overall, approximately 40% of phosphoproteins containing ERK substrate motifs were shared between mouse and human cells with *Jak2* mutations (Extended Data Fig. 9c). Of these, MKNK1 and MCL-1 were identified as relevant ERK targets (Fig. 4c). To confirm these effects on cell signalling, we investigated JAK2-dependent pathways in the presence or absence of pharmacologic treatment with JAK inhibitor. Inactivation of YBX1

again led to a considerable reduction of ERK phosphorylation in both mouse and human cells (Fig. 4d and Extended Data Fig. 9d–f), whereas STAT signalling was largely unaffected. Concomitant pharmacologic JAK inhibition abrogated ERK signalling, while decreasing STAT signalling, irrespective of YBX1 inactivation. Thus, YBX1 is required for the maintenance of ERK signalling downstream of JAK2VF. Genetic inactivation of *Mknk1* by RNAi likewise abrogated ERK signalling and sensitized the cells to cell death induced by JAK inhibitor (Extended Data Fig. 9g–j), linking YBX1-dependent expression of *Mknk1* to the maintenance of ERK signalling in JAK2VF cells. Besides RNA splicing and processing, disturbed cellular functions indicated by proteome changes in YBX1-depleted JAK2VF cells included positive regulation of programmed cell death and apoptosis (Extended Data Fig. 10a). Supporting this, RNAi inactivation of *Ybx1* in JAK2VF cells reduced phosphorylation of MCL-1 (Extended Data Fig. 10b, c). Likewise, YBX1 loss concomitantly decreased abundance of MCL-1 and induction of BIM in a gene-dose dependent manner (Extended Data Fig. 10d), and induction of apoptosis after YBX1 knockdown and JAK inhibitor treatment could be rescued by forced expression of MCL-1 (Extended Data Fig. 10e).

Finally, pharmacological modulation of MKNK1 or ERK signalling in combination with treatment with two different JAK inhibitors induced

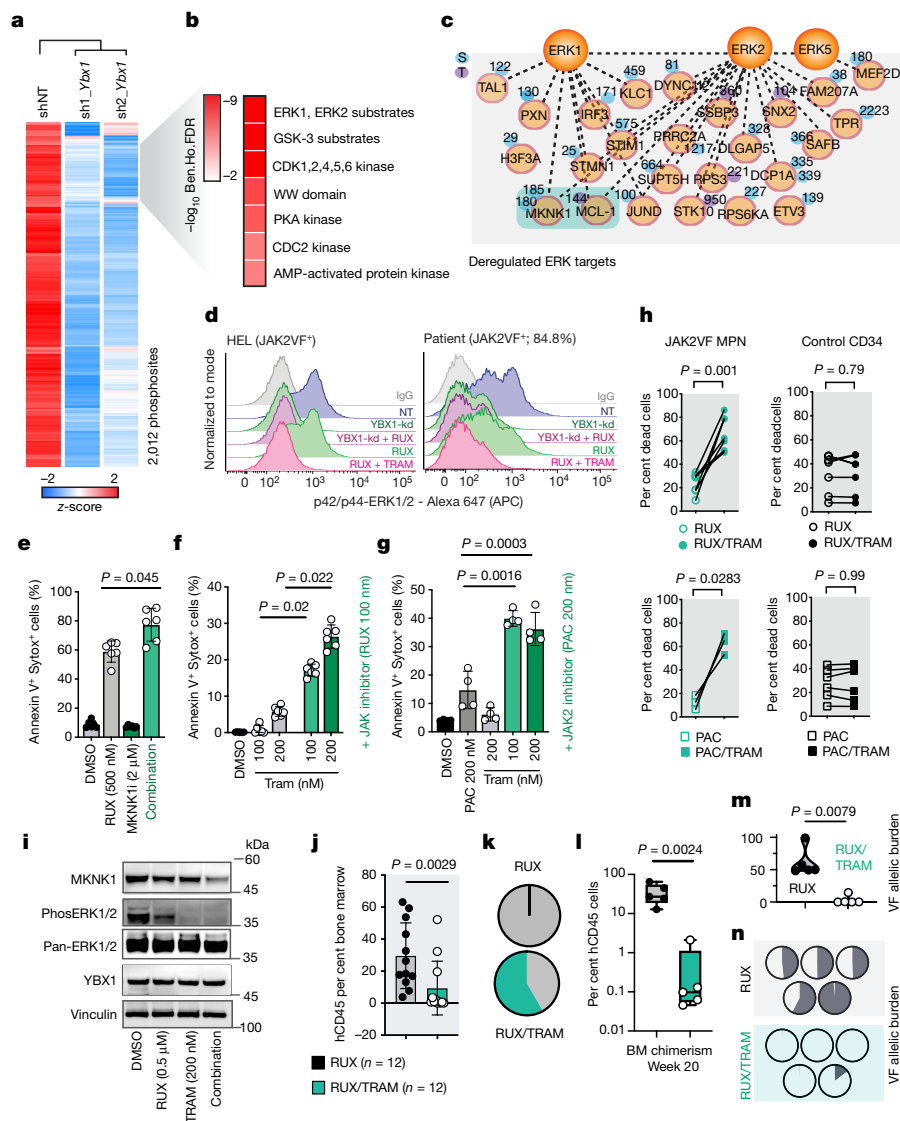


**Fig. 4 | *Jak2*-mutated clones are selectively vulnerable to inhibition of ERK signalling.** **a**, Unsupervised hierarchical clustering of 2,012 significantly downregulated phosphosites in *Ybx1*-targeted, *Jak2*-mutated mouse cells (two shRNAs) and non-targeting control (shNT). Averaged replicates ( $n = 4$ ); heatmap shows z-scored  $\log_2$ -transformed phosphosite intensity. **b**, Kinase substrate motifs significantly downregulated in *Ybx1*-targeted *JAK2VF* cells ( $-\log_{10}$  Benjamini–Hochberg FDR value). **c**, Network map: proteins assigned as ERK substrates (significantly downregulated phosphoserine (blue) and phosphothreonine (purple) residues, indicated by position). **a**, **c**, ANOVA, permutation-based FDR < 0.01. **d**, Representative flow cytometry histograms showing pERK levels in *JAK2*-mutated HEL (left) and primary patient cells (right) after RNAi (shNT; sh*Ybx1*) and/or drug treatment (500 nM JAK inhibitor (ruxolitinib, RUX) or 200 nM MEK/ERK inhibitor (trametinib, TRAM)). **e–g**, Pharmacologic inhibition of mouse *JAK2VF* cells with ruxolitinib alone or with MKNK1 inhibitor (CGP57380, MKNK1-i; 2  $\mu$ M;  $n = 6$ , mean  $\pm$  s.d.; **e**), ruxolitinib alone or with trametinib (100, 200 nM;  $n = 6$ , mean  $\pm$  s.d.; **f**) or the *JAK2* inhibitor pacritinib (PAC) alone or with trametinib (100, 200 nM;  $n = 4$ , mean  $\pm$  s.d.; **g**), as indicated by percentage of apoptotic (annexin V<sup>+</sup> Sytox<sup>+</sup>) cells. **h**, Proportion of dead cells in FACS-sorted CD34<sup>+</sup> *JAK2VF*<sup>+</sup> MPN bone marrow cells ( $n = 6$ ) and

non-malignant CD34<sup>+</sup> controls ( $n = 6$ ) treated with ruxolitinib (500 nM), pacritinib (200 nM) or either plus trametinib (200 nM). **i**, Representative western blot (of  $n = 3$ ) showing reduction of MKNK1 protein abundance in HEL cells following ruxolitinib + trametinib treatment. **j**, **k**, Xenograft model using NSGS mice transplanted with *JAK2VF*<sup>+</sup> HEL cells and treated with ruxolitinib ( $n = 12$ ) or ruxolitinib + trametinib ( $n = 12$ ). **j**, Percentages of hCD45<sup>+</sup> bone marrow cells ( $n = 12$  per cohort; mean  $\pm$  s.d.). **k**, Disease penetrance (%) in NSGS animals: hCD45 positivity (>1%, grey) or negativity (<1%, green) after ruxolitinib or ruxolitinib + trametinib treatment, respectively. **l–n**, Patient-derived xenograft (PDX) model to investigate primary *JAK2VF*<sup>+</sup> bone marrow cells from three different patient donors in human mice (NSGW41). Recipient animals were treated with ruxolitinib (90 mg kg<sup>-1</sup> twice a day) or ruxolitinib + trametinib (1 mg kg<sup>-1</sup> once a day by gavage for 5 d every 4 weeks). **l**, Bone marrow analysis of human cell chimerism in week 20 ( $n = 5$  per cohort). Box plots shows mean  $\pm$  s.d. with minimum and maximum. **m**, Quantification of *JAK2V617F* allelic burden by pyrosequencing in sorted hCD45<sup>+</sup> bone marrow cells of recipient animals. **d–m**, *P* values (two-tailed *t*-test. **n**, Pie charts of *JAK2V617F* allelic burden per individual for mice treated with ruxolitinib (grey) or ruxolitinib + trametinib (green). In **d–n**, *n* indicates independent biological replicates.

apoptosis in mouse (Fig. 4e–g) and primary human *JAK2VF*-mutated CD34<sup>+</sup> bone marrow cells but not in CD34<sup>+</sup> bone marrow from healthy human control donors (Fig. 4h). This therapeutic combination of *JAK2* and ERK inhibition markedly downregulated MKNK1 levels in both mouse and human cells, indicating that MKNK1 is the primary target of this combination (Fig. 4i and Extended Data Fig. 10f). Likewise, treating

human *JAK2VF*-mutated cell-lines with a combination of *JAK* inhibitor and the ERK inhibitor trametinib in a xenograft model reduced persistent cells (Fig. 4j) and disease penetrance in vivo (Fig. 4k). These findings were confirmed using primary human *JAK2VF*-mutated bone marrow cells in a patient-derived xenograft (PDX) model of MPN. Here, in vivo treatment with a combination of *JAK* and ERK inhibitors after

engraftment of human cells resulted in a significant decrease of hCD45 peripheral blood (Extended Data Fig. 10g) and bone marrow chimerism (Fig. 4l) and abrogated the JAK2VF clone in two of five recipients, as confirmed by pyrosequencing of FACS-isolated hCD45 cells (Fig. 4m, n). To further confirm ERK as a relevant target in *JAK2* mutant cells, we performed in-depth phosphoproteome analysis of primary human *JAK2*-mutated cells exposed in vitro or in vivo to JAK inhibitor. JAK inhibitor treatment significantly altered 618 phosphosites, including those of relevant mRNA splicing factors (Extended Data Fig. 10h, i). Consistent with our previous findings, JAK inhibitor treatment did not greatly alter MAPK phosphorylation (Extended Data Fig. 10j) but did affect NF- $\kappa$ B and STAT signalling (Extended Data Fig. 10k).

Many cancers harbouring mutated kinases can be targeted with kinase inhibitors because of their inherent dependency on this oncogenic hit. However, JAK inhibitors do not eliminate JAK-mutated clones, which has restricted their use to symptom-oriented therapeutic approaches<sup>2</sup>. As a result of an oncogenic mutation, cancer cells may also develop secondary dependency on pathways or molecules that are not originally oncogenic<sup>14</sup>. Using in-depth phosphoproteomic analysis, our data provide a first unbiased and global view on relevant downstream effectors of mutant *JAK2*. We identified phosphorylation of YBX1 by mutated *Jak2* as a critical event required for *Mknk1* mRNA splicing. MKNK1 is an essential component of ERK signalling and required for the maintenance of *Jak2*-mutated cells during treatment with JAK inhibitor, revealing an important regulatory mechanism of disease persistence. Although recent studies have highlighted the role of ERK signalling in *Jak2*-mutated cells<sup>15–17</sup>, we here discover how cell-intrinsic mechanisms of differential protein phosphorylation can result in splicing-dependent alterations of cell signalling (Extended Data Fig. 10l). Direct and specific inhibitors of YBX1 are not available for clinical use so far, but identification of relevant protein domains using genetic screens may facilitate such developments in the future. Confirmation of dual JAK2 and ERK targeting using primary cells in vivo establishes a therapeutic principle for neoplasms carrying mutations in *JAK2* and a strong experimental rationale for incorporating the JAK2–YBX1-mediated regulation of MKNK1-dependent ERK signalling into therapies directed at the elimination of the persistent *JAK2*-mutated clone.

## Online content

Any methods, additional references, Nature Research reporting summaries, source data, extended data, supplementary information, acknowledgements, peer review information; details of author contributions and competing interests; and statements of data and code availability are available at <https://doi.org/10.1038/s41586-020-2968-3>.

1. Darnell, J. E., Jr, Kerr, I. M. & Stark, G. R. Jak-STAT pathways and transcriptional activation in response to IFNs and other extracellular signaling proteins. *Science* **264**, 1415–1421 (1994).
2. Perner, F., Perner, C., Ernst, T. & Heidele, F. H. Roles of JAK2 in aging, inflammation, hematopoiesis and malignant transformation. *Cells* **8**, 854 (2019).
3. Genovese, G. et al. Clonal hematopoiesis and blood-cancer risk inferred from blood DNA sequence. *N. Engl. J. Med.* **371**, 2477–2487 (2014).
4. Jaiswal, S. et al. Age-related clonal hematopoiesis associated with adverse outcomes. *N. Engl. J. Med.* **371**, 2488–2498 (2014).
5. Forbes, S. A. et al. COSMIC: somatic cancer genetics at high-resolution. *Nucleic Acids Res.* **45** (D1), D777–D783 (2017).
6. Deininger, M. et al. The effect of long-term ruxolitinib treatment on JAK2p.V617F allele burden in patients with myelofibrosis. *Blood* **126**, 1551–1554 (2015).
7. Harrison, C. N. et al. Long-term findings from COMFORT-II, a phase 3 study of ruxolitinib vs best available therapy for myelofibrosis. *Leukemia* **30**, 1701–1707 (2016).
8. Humphrey, S. J., Azimifar, S. B. & Mann, M. High-throughput phosphoproteomics reveals in vivo insulin signaling dynamics. *Nat. Biotechnol.* **33**, 990–995 (2015).
9. Hsu, T. Y. et al. The spliceosome is a therapeutic vulnerability in MYC-driven cancer. *Nature* **525**, 384–388 (2015).
10. Climente-González, H., Porta-Pardo, E., Godzik, A. & Eyras, E. The functional impact of alternative splicing in cancer. *Cell Rep.* **20**, 2215–2226 (2017).
11. Dolfini, D. & Mantovani, R. YB-1 (YBX1) does not bind to Y/CCAAT boxes in vivo. *Oncogene* **32**, 4189–4190 (2013).
12. Stickeler, E. et al. The RNA binding protein YB-1 binds A/C-rich exon enhancers and stimulates splicing of the CD44 alternative exon v4. *EMBO J.* **20**, 3821–3830 (2001).
13. Wei, W. J. et al. YB-1 binds to CAUC motifs and stimulates exon inclusion by enhancing the recruitment of U2AF to weak polypyrimidine tracts. *Nucleic Acids Res.* **40**, 8622–8636 (2012).
14. Kaelin, W. G., Jr. The concept of synthetic lethality in the context of anticancer therapy. *Nat. Rev. Cancer* **5**, 689–698 (2005).
15. McCubrey, J. A. et al. Involvement of p53 and Raf/MEK/ERK pathways in hematopoietic drug resistance. *Leukemia* **22**, 2080–2090 (2008).
16. Meyer, S. C. Mechanisms of resistance to JAK2 inhibitors in myeloproliferative neoplasms. *Hematol. Oncol. Clin. North Am.* **31**, 627–642 (2017).
17. Stivala, S. et al. Targeting compensatory MEK/ERK activation increases JAK inhibitor efficacy in myeloproliferative neoplasms. *J. Clin. Invest.* **129**, 1596–1611 (2019).

**Publisher's note** Springer Nature remains neutral with regard to jurisdictional claims in published maps and institutional affiliations.

© The Author(s), under exclusive licence to Springer Nature Limited 2020

# Article

## Methods

### Cell culture

Mouse Ba/F3 cells stably expressing JAK2WT and JAK2VF, human SET-2 and HEL cells (purchased from and authenticated by DSMZ, Braunschweig, Germany) were cultured in RPMI1640 medium (Life Technologies, Carlsbad, CA, USA) supplemented with 10% FBS (Life Technologies). HEK293T cells (purchased and authenticated from DSMZ) were cultured in DMEM + GlutaMAX medium (Life Technologies) supplemented with 10% FBS (Life Technologies). All cell lines were maintained in a humidified atmosphere with 5% CO<sub>2</sub> at 37 °C. Cell lines were tested and maintained mycoplasma free throughout the study. Primary mouse and human cells were cultured in StemSpan SFEM medium (StemCell Technologies, Vancouver, Canada) supplemented with cytokines (mouse: 100 ng/ml mSCF, 10 ng/ml mTPO, 6 ng/ml mL-3 and 10 ng/ml mL-6; human: hFLT3 100 ng/ml, hSCF 50 ng/ml, hIL-6 10 ng/ml, hIL-3 6 ng/ml; all Pepro Tech, Rocky Hill, NJ, USA).

### Primary patient samples

All types of patient samples and healthy donor controls derived during routine biopsies (peripheral blood, bone marrow aspirates and biopsies) and investigated in this study were obtained after informed consent and according to the Helsinki declaration from the Tumour Banks in Jena and Magdeburg. Scientific protocol, patient information and patient approval forms have been approved by the respective local ethics committees ('Ethics Committee, University Hospital Jena' no. 4753/04-16 and 'Ethics Committee, Medical Faculty, OvGU Magdeburg' no. 115/08).

### Focused lentiviral shRNA library screen

In brief, the Mission TRC lentiviral pLKO.1 shRNA vectors from Sigma targeting the top15 hits of mRNA processing and splicing factors enriched in JAK2VF were selected (in total 74 shRNAs, 4–5 different shRNAs per hit and 4 non-targeting controls; the shRNA sequences are provided in Supplementary Table 1) and lentiviruses were individually produced per shRNA by co-transfecting with the 3<sup>rd</sup> generation packaging plasmids pMDL, pRSV and pVSVG in HEK293T cells seeded in 10 cm culture dishes. The viruses were collected at 48 and 72 h after transfection, syringe filtered through a 0.45- $\mu$ m syringe filters and concentrated using 30K Amicon Ultra-15 centrifugal filters (Merck), and the target mouse Ba/F3 JAK2V617F cells were infected with polybrene (8 mg/ml, Sigma). For screening purposes, 200,000 mouse Ba/F3 JAK2V617F cells in 2 ml RPMI media with 10% hiFBS were seeded in each well of a six-well plate. Concentrated virus was added per well (with polybrene 8 mg/ml), centrifuged at 500  $\times$  g for 1 h at 35 °C, and subsequently 48 h after transduction cells were selected with 1  $\mu$ g/ml puromycin for 2 d. On day 3, cells were washed, and viable cells were counted and plated in 96 well plates (8 technical replicates per sample condition per experiment; in addition, each experiment was performed as technical duplicates) for growth assay with and without the JAK2 inhibitor ruxolitinib (RUX; 0.5  $\mu$ M). The plates were incubated at 37 °C and 5% CO<sub>2</sub> for 72 h and subjected to Cell Titer 96 Aqueous One solution (Promega) according to the manufacturers' protocol. To each well, 20  $\mu$ l MTS solution was added, the plates were incubated for 4 h and absorbance was recorded at 490 nm with a 96-well plate reader. Further viable cells were counted after 72 h with the Countess automated cell counter (Thermo Fischer Scientific) using trypan blue. Western blotting was carried out to assess knock down efficiency on protein level for PCBP1 (Abcam, ab168378, dilution 1:1,000) and YBX1 (Abcam, ab76149, dilution 1:1,000). For data analysis, the 8 technical duplicates were averaged and the values were normalized against non-targeting controls included in each plates. The analysis of the normalized data between biological replicates showed correlation coefficient between  $r = 0.963$  and  $0.988$ , indicating high reproducibility of the procedure. Targets were considered potential candidates if two or more shRNA responded only in the JAK2 inhibitor

treated group but not in the untreated controls of all the biological replicate experiments performed. Using these criteria, we choose our candidates for further characterization.

### Genetic inactivation of mouse and human YBX1 by RNAi

To target YBX1, 4 mouse and 5 human shRNAs targeting *Ybx1* (all received from Sigma-Aldrich, St. Louis, MO, USA) were validated and two selected shRNAs were used thereafter (mentioned in the supplementary shRNA table) with respective non-targeting controls. In brief, Ba/F3, SET-2 and HEL cells were lentiviral transduced with lentiviral particles by spinfection (872  $\times$  g for 1.5 h at 33 °C). The cells were cultured for 2 d, puromycin selected for 48 h and seeded ( $5 \times 10^6$  cells), and then subjected to inhibitor treatment or addition of diluent control as indicated below. Cells were harvested and YBX1 knockdown was analysed by qPCR and western blotting.

### Assessment of cell growth and viability dependence on JAK inhibitor dose

shNT control or sh*Ybx1*/sh*Mknk1* (two different shRNAs targeting *Ybx1* and *Mknk1*)-targeted mouse Ba/F3 JAK2VF cells were counted with the Countess automated cell counter (Thermo Fischer Scientific) using trypan blue cell viability in 96 well plates for viable cells after 2 d of 1  $\mu$ g/ml puromycin selection.  $3 \times 10^4$  viable cells per well (8 technical replicates per row per sample condition) in 96 well plates were seeded in RPMI medium with 10% hi-FBS exposed to different concentrations of the JAK inhibitor RUX ranging from 1 nM to 10  $\mu$ M. The plates were incubated at 37 °C and 5% CO<sub>2</sub> for 72 h and subjected to Cell Titer 96 Aqueous One Solution (Promega) according to the manufacturer's protocol. Viable cells were counted after 72 h by trypan blue exclusion. IC<sub>50</sub> inhibitory concentration of RUX was calculated using GraphPad Prism.

### Drug combination treatments

Viable Ba/F3 JAK2VF cells were seeded at a density of 30,000 cells per well in RPMI medium with 10% heat inactivated FBS (Invitrogen) and exposed to JAK inhibitor (0.5  $\mu$ M RUX) alone or in combination with different concentrations of the MKNK1 inhibitor CGP57380 (Sigma), the MEK/ERK inhibitor trametinib (Novartis), the PI3K inhibitor LY294002 and the p38 inhibitor SB203580 (Merck) and incubated for 72 h. Cell Titer 96 Aqueous One Solution was added to the plates according to the manufacturers' protocols and measurements were performed after 4 h. The plates were read at 490 nm in Tecan Infinite M200 and the response were analysed using GraphPad Prism.

### Apoptosis assays

Cells stably infected with either non-targeting or target-specific (*Ybx1*, *Mknk1*) shRNAs were seeded in six-well plates and selected for 24 h with puromycin. Primary mouse lineage-depleted cells or FACS-sorted human CD34<sup>+</sup> cells were incubated in 48 well plates. Inhibitor treatment was performed at concentrations as indicated for 48 h unless otherwise stated. Apoptosis was measured by flow cytometry on a BD FACSCanto cytometer using Annexin V (1:50 dilution) in combination with SYTOX Blue or SYTOX Green or 7AAD as dead cell stains.

### Proliferation assay with PCNA

After puromycin selection of shNT and sh*Ybx1* mouse Ba/F3 JAK2VF cells, they were washed in ice-cold 1 $\times$  PBS twice, fixed in 70% ethanol and permeabilized with 0.1% Tween-20. Cells were stained for PCNA–Alexa Fluor 488 conjugate (Biozol) on ice for 20 min.

### Cell cycle analysis

For cell cycle measurements,  $2 \times 10^6$  mouse Ba/F3 JAK2VF cells expressing shNT or sh*Ybx1* were washed in ice-cold 1 $\times$  PBS twice, fixed in ice cold 70% ethanol for 30 min on ice and stored at 4 °C. After collection of biological replicates, samples were ribonuclease A treated and stained with propidium iodide. The PI-stained cells were measured using a



BD FACSCantoII cytometer and the data were analysed using FlowJo software (Treestar, Ashland, OR, USA).

### ROS measurements using Carboxy-H<sub>2</sub>DFFDA

In brief,  $1 \times 10^6$  mouse Ba/F3 JAK2VF cells stably expressing shNT or sh*Ybx1* were washed in  $1 \times$  PBS twice and resuspended in  $20 \mu\text{M}$  carboxy-H<sub>2</sub>DFFDA for 30 min in dark at room temperature. Further the cells were washed in  $1 \times$  PBS thrice and measured using BD FACSCanto cytometer. Data were analysed in FlowJo.

### DNA damage analysis using $\gamma$ H2AX pS139

$1 \times 10^6$  mouse Ba/F3 JAK2VF cells stably expressing shNT or sh*Ybx1* cells were seeded on poly-L-lysine coated dishes for 2–4 h, washed in PBS, fixed with 4% paraformaldehyde, blocked in blocking buffer (0.2% Triton-X, 1% BSA and 5% normal rabbit serum) and incubated overnight with rabbit  $\gamma$ H2AX pS139 antibody (Cell Signaling, 2577, 1:800) overnight. After overnight incubation, samples were washed and incubated with secondary antibody (anti-rabbit-Alexa 568). DAPI was used for nuclear staining (NucBlue, ThermoScientific). Positive control samples were prepared by exposing the Ba/F3 JAK2VF cells expressing shNT to 20 min UV under the cell culture hood. Imaging was performed using Zeiss LSM 780 microscope and processed in Zen Black software tool.

### Preparation of label-free phosphoproteome samples

Samples were processed according to the protocol previously described<sup>8</sup>. In brief, samples were collected as quadruplicate biological replicates for each condition, lysed in Gmdcl buffer (6 M Gmdcl, 100 mM Tris, pH 8.5, 10 mM TCEP and 40 mM CAA), heated for 5 min at 95 °C and cooled on ice for 15 min. Lysed samples were then sonicated (Branson probe sonifier output 3–4, 50% duty cycle,  $10 \times 30$  s) and heated again. Proteins were precipitated with acetone and quantified by BCA assay. 2 mg was digested with LysC and trypsin overnight at room temperature and phosphopeptides enriched using TiO<sub>2</sub> beads. The enriched peptides were desalted, washed and eluted on StageTips with 2 layers of SDB-RPS material with elution buffer (80% acetonitrile (ACN) and 5% NH<sub>4</sub>OH). The eluted peptides were vacuum centrifuged until dryness and reconstituted in 2% ACN/0.1% TFA. All the samples were stored at –20 °C until measurement.

### Phosphoproteome of primary patient samples

In brief, peripheral blood samples from patients with *JAK2*-mutated myeloproliferative neoplasms were collected, granulocytes isolated, and treated with DMSO or RUX  $0.5 \mu\text{M}$  for 2 h in vitro. Also, for in vivo exposure, cells were isolated from patients with MPN before and 2 h after dosing of RUX (10 mg to 20 mg oral dose during routine treatment). Cells were lysed and processed in 4% SDC buffer (4% SDC, 100 mM Tris pH 8.5, 10 mM TCEP and 40 mM CAA), heated for 5 min at 95 °C and cooled on ice for 15 min. Lysed samples were sonicated, heated again for 5 min and BCA quantified. Approximately 350  $\mu\text{g}$  of proteins was digested with LysC and trypsin overnight at room temperature and phosphopeptides were enriched using TiO<sub>2</sub> beads as described elsewhere<sup>18</sup>.

### Deep proteome quantification

Cell were lysed and peptides were prepared as previously described<sup>19</sup>. Proteome samples of phosphoproteome analysis were collected after TiO<sub>2</sub> enrichment. In brief, cells were lysed in 1% SDC buffer (1% SDC, 100 mM Tris, pH 8.0, 40 mM CAA and 10 mM TCEP), heated for 5 min at 95 °C, cooled on ice for 15 min and sonicated (Branson probe sonifier output 3–4, 50% duty cycle,  $10 \times 30$  s). 25  $\mu\text{g}$  was digested with LysC and trypsin overnight, and peptides were eluted on Stage Tips with three layers of SDB-RPS material with elution buffer. The eluted peptides were vacuum centrifuged until dryness and reconstituted in 2% ACN/0.1% TFA. All the samples were stored in –20 °C until measurement.

### Drug-perturbed phosphoproteome profiling

To profile the actions of kinase inhibitors on JAK2VF, Ba/F3-expressing mouse JAK2VF cells were treated with  $0.5 \mu\text{M}$  of the JAK2 inhibitor RUX (Selleckchem, S1378) for 2 h and with  $10 \mu\text{M}$  of the MEK inhibitor PD0325901 (Sigma),  $10 \mu\text{M}$  of the p38 inhibitor SB203580 (Merck),  $20 \mu\text{M}$  of the JNK inhibitor SP600125 (Sigma),  $50 \mu\text{M}$  of the PI3K inhibitor LY294002 (Merck),  $10 \mu\text{M}$  of the AKT inhibitor MK2206 (Enzo Life) and 100 nM of mTOR inhibitor Torin-1 (Millipore) for 1 h. The cells were lysed in Gmdcl buffer and processed as described for phosphoproteome sample preparation.

### YBX1 interactome preparation

For YBX1 affinity purification, cells were lysed in 150 mM NaCl, 50 mM Tris (pH 7.5), 5% glycerol, 1% IGPAL-CA-630 (Sigma), protease inhibitors (EDTA free, Roche), 1% Benzozonase and 1 mM MgCl<sub>2</sub> for 30 min on ice. 1 mg of total lysate was precleared with protein A Sepharose beads, incubated with validated YBX1 antibody (Abcam ab76149) overnight and 30  $\mu\text{l}$  of rec-protein A Sepharose 4B conjugates (Invitrogen) for 2 h. Non-specific binders were removed by three washes with wash buffer I (150 mM NaCl, 50 mM Tris (pH 7.5), 5% glycerol, 0.05% IGPAL-CA-630) and three washes with wash buffer II (150 mM NaCl, 50 mM Tris (pH 7.5)). The bound proteins were on-beads digested with Trypsin and LysC overnight. The peptides were desalted on C<sub>18</sub> Stage tips and analysed by mass spectrometry.

### Liquid chromatography (LC)–MS/MS measurement

For the LC–MS/MS analysis, Q-Exactive mass spectrometer with a nano-spray ion source connected online to an Easy-nLC 1000 HPLC system was used. Peptides were separated on an in-house-prepared 50-cm C<sub>18</sub> columns (75  $\mu\text{m}$  inner diameter with 1.9  $\mu\text{m}$  C<sub>18</sub> ReproSil particle, Dr. Maisch GmbH) in a 140 min gradient from 5–65% in buffer B (0.5% formic acid, 80% acetonitrile). The column temperature was maintained at 50 °C using a column oven (in-house made). Peptides were analysed with a full scan ( $300$ – $1,600$   $m/z$ ,  $R = 60,000$  at  $200$   $m/z$ ) at a target of 3e6 ions, followed by high energy collisional disassociation-based fragmentation (HCD) of top10 most abundant isotope patterns with a charge  $\geq 2$  MS/MS scan, detected in the Orbitrap detector ( $R = 15,000$  at  $200$   $m/z$ ). Dynamic exclusion of sequenced peptides was set to 40 s and apex trigger (4–7 s) was on. All data were acquired using X-caliber software (Thermo Scientific).

### Data processing with Maxquant

Mass spectrometric raw files were processed using the Andromeda search engine integrated into Maxquant<sup>20</sup> environment (1.5.5.2 version). The MS/MS spectra were matched against the mouse (UniProt FASTA 2015\_08) database with an FDR < 0.01 at the level of proteins, peptides and modifications. The search included fixed modification for carbamidomethyl and in the variable modifications table phosphoSTY was added additionally for the phosphorylated peptide search to the default settings. Peptides with at least seven amino acids were considered for identification. Maximum two missed cleavages were allowed for protease digestion. Match between run was enabled with the matching window of 1 min to transfer peptide identification to across runs based on normalized retention time and high mass accuracy.

### Phosphoproteome data analysis

A Perseus<sup>21</sup> (version 1.5.2.11) software environment was used for all Maxquant output table analysis. For phosphoproteome analysis, sample for class I phosphosites (localization probability > 0.75) and required a minimum of 3 or 4 valid values in each of the biological quadruplicates. Statistical analysis was performed on the logarithmized intensities values. Significance was assessed by Student's *t*-test using permutation-based FDR, to identify the significantly regulated phosphosites. In group comparisons a two-sample *t*-test or, for multiple samples, a comparison

## Article

ANOVA test was performed with permutation-based FDR cut-off 0.01 or 0.05. The significantly regulated phosphosites were filtered, *z*-scored and represented as either unsupervised hierarchical clustered heat maps or profile plots. Annotations were extracted from UniprotKB, Gene Ontology (GO), the Kyoto Encyclopedia of Genes and Genomes (KEGG) and Reactome. Kinase-substrates relationships and kinase motifs were extracted from the PhosphoSitePlus database (phosphosite.org). Fisher's exact test was performed to discover motifs and annotations that are significantly regulated in the sample groups. For phosphosite occupancy calculation, the proteomes and phosphoproteomes of corresponding samples were matched in maxquant to estimate occupancy, occupancy ratio and occupancy error scale using the extracted signal difference of modified peptide, unmodified peptide and the corresponding protein ratios (described earlier<sup>8</sup>). Phosphoprotein network architecture were obtained using String database and further networks and sub-networks were analysed and visualized in Cytoscape (version 3.5.1).

### RNA sequencing and ChIP sequencing

Transcriptome profiling of Ba/F3 JAK2V617F cells transduced with shNT or sh*Ybx1* cells was performed using a strand-specific RNA sequencing protocol. In brief, total RNA was isolated from  $2 \times 10^6$  cells using a NucleoSpin RNA Kit according to the manufacturers' protocol (Macherey Nagel). An RNA library for sequencing was prepared using NEBNext Poly(A) mRNA Magnetic Isolation Module. The quality was analysed on a Bioanalyzer (Agilent 2100 Bioanalyzer) high sensitivity DNA assay. Samples were sequenced on Illumina Nexseq500 and multiplexed reads were demultiplexed on the basis of their barcodes. Sequencing reads were filtered, trimmed and then mapped to the Ensembl gene annotation and the mouse genome assembly GRCm38 using STAR aligner<sup>22</sup> with ENCODE settings in two-pass mode considering splice junctions across all samples in the second mapping step. Gene counts were quantified using *featureCounts*<sup>23</sup> and differential expression calculated with the *limma-voom* pipeline<sup>24</sup>. Gene and transcript expression levels were quantified using RSEM. Event level differential splicing was calculated with the *EventPointer* package<sup>25</sup> in R. Chromatin immunoprecipitation (ChIP) was performed using a ChIP-validated YBX1 antibody (Abcam #76149). Cells were crosslinked (1% formaldehyde, 10 min) and nuclei were isolated, lysed and sonicated to yield chromatin fragments of about 200–500 bp. Chromatin was diluted with ChIP buffer, pre-cleared with Protein A/G Sepharose that had been blocked with 1 mg/ml BSA and 1% gelatin from cold water fish skin. Chromatin from  $5 \times 10^6$  cells was incubated with 5  $\mu$ g anti-YBX1 antibody overnight followed by immobilization on Sepharose. After extensive washing, immunoprecipitated material was eluted with 1% SDS/0.1 M NaHCO<sub>3</sub> and chromatin was de-crosslinked (65 °C, 6 h)<sup>26</sup>. ChIP-sequencing libraries were prepared using the ThruPLEX DNA-library kit (Takara) and sequenced on an Illumina NextSeq platform. To remove the adaptors and low-quality parts of DNA reads trimming was done using FASTX-Toolkit (Quality threshold was specified as 20 and the minimum length of trimmed reads is 1, version 0.0.14) and TrimGalore (version 0.4.4). After trimming, the DNA read mapping to reference sequences is performed by Segemehl with default parameters (version 0.2.0-418). Samtools (version 0.1.19) was used for conversion from SAM format to BAM format. Reads were aligned using Bowtie 2 (version 2.4.0). For peak calling, MACS2 (version 2.1.1) was applied, and *Q* value is assigned as 0.01. HOMER (version 4.11) was used for call motifs. Analysis was performed using Basepair software tool default settings (version 3).

### In vitro transcription

Intron retained *Mknk1* region (exon 12–exon13) was cloned with T7 promoter. Biotin labelled *Mknk1* mini pre-mRNAs (biotin-11-dUTP, Cat# NU-803-BIOX, Jena Bioscience) was in vitro transcribed at 37 °C for 4 h using MegaScript T7 RNA polymerase (AM1333, Thermo Fisher) with 10:1 ratio of Ribo m7G Cap Analogue to GTP (P171A, Promega), DNase I

treated for 15 min at 37 °C and then subjected to RNA purification using NucleoSpin RNA columns (Cat#740955, Macherey-Nagel).

### In vitro splicing assay

Nuclear extract from Ba/F3 JAK2V617F cells with and without *Ybx1* expression owing to shRNA targeting was prepared and splicing assay was performed as described elsewhere<sup>27</sup>. Briefly, splicing reaction of 25  $\mu$ l contained 50  $\mu$ g of nuclear extract, 10 nM RNA substrate, 1 nM DTT, 3.7% polyvinyl alcohol (low molecular weight, Sigma), 1 mM magnesium acetate, 1.7 mM ATP, 17 mM phosphocreatine, 20 mM glycine, 2.5  $\mu$ l (10 U) RNasin Plus (Promega). Splicing reaction was incubated at 30 °C for 2 h; reaction was stopped by adding Proteinase K for 30 min at 45 °C followed by streptavidin pull-down of biotinylated RNA. The purified RNA was reverse transcribed using RevertAid first-strand cDNA synthesis protocol using random hexamer as primers (Cat# K1621, Thermo Scientific), PCR was performed with the *Mknk1* primers forward 5'-AACAAAGCTGTTTGAGAGCATCCAG-3' and reverse 5'-CTCTGAAGGACTTGC GGCGTG-3', and the products were resolved in an agarose gel and visualized with SafeRed gel staining.

### Genetic inactivation by genome editing using CRISPR/Cas9

Guide RNAs targeting *Ybx1* were designed using the Broad GPP tool and sequences of sgRNAs are provided in Supplementary Table 1. For cloning of sgRNA sequences, the improved-scaffold-pU6-sgRNA-E F1Alpha-PURO-T2A-RFP (ipUSEPR) vector system<sup>28</sup> with puromycin resistance and RFP selection marker was used (kindly provided by S. Armstrong, Department of Paediatric Oncology, Dana Farber Cancer Institute, Harvard University, Boston, MA, USA). HEK293T cells were transfected using FUGENE HD Transfection Reagent (Promega) to generate lentiviral particles as described above. Ba/F3 JAK2V617F-GFP\_Cas9-Blast cells were infected twice (8 h gap in between) by spinfection (872g, 1.5 h, 33 °C). The cells expressing sgRNAs were selected with 1  $\mu$ g/ml puromycin starting on day 2 post-infection. For knockout confirmation, cells were collected for RT-qPCR or western blotting on day 8 post-infection.

### NMD and spliceosome machinery inhibition

For treatment with inhibitors of nonsense-mediated decay (NMD), Ba/F3 JAK2V617F\_Cas9 cells transduced with either sgLuc or 2 different sgRNAs targeting *Ybx1* were treated with Dorsomorphin (Compound C; 10  $\mu$ M, 24 h; Abcam, Cambridge, UK) or VG-1 (5  $\mu$ M, 10  $\mu$ M, 20 h), respectively. DMSO treated cells were used as a control. For inhibition of splicing machinery, Ba/F3 JAK2V617F cells were treated with either pladienolide B (10 nM, 8 h; Santa Cruz Biotechnologies, Dallas, TX, USA) or herboxidiene (25 nM, 8 h; Cayman Chemical, Ann Arbor, MI, USA), respectively. DMSO treated cells were used as a control.

### Mouse genotyping

Genotyping of tails from conditional *Ybx1* knockout mice was performed using the following primers: *Ybx1\_cond\_for* (GCCTAAGGATAGT-GAAGTTTCTGG), *Ybx1\_con\_rev* (CCTAGCACACCTTAATCTACAGCC); *Cre\_for* (CGTATAGCCGAAATTGCCAG), *Cre\_rev* (CAAAACAGGTAGT-TATTCCG). Genotyping PCR was performed using the Dream Taq Green PCR Master Mix (2 $\times$ ) (Thermo Fisher Scientific, Waltham, MA, USA) following the manufacturers' protocol.

### Histology staining and immunohistochemistry

Formalin-fixed and paraffin-embedded bone marrow biopsies with proven myeloproliferative neoplasia or primary samples without histopathologic abnormalities were retrieved from the archival files of the Institute of Pathology, Otto von Guericke University Medical Center, Magdeburg, Germany. All MPNs were diagnosed and classified according to the World Health Organization (WHO) 2008 classification in synopsis with clinical data and presentation. The study comprises of biopsies derived from 76 patients with MPN (PV (*n* = 23), ET (*n* = 32) and

MF ( $n = 21$ ) compared to healthy donor controls ( $n = 18$ ) or BCR-ABL positive CML ( $n = 17$ ). Immunohistochemistry was performed using a monoclonal Rabbit-anti-human YBX1 antibody (Abcam; ab76149) in a dilution of 1:100. Spleen, liver and lung from *Ybx1<sup>+/+</sup>* JAK2VF and *Ybx1<sup>-/-</sup>* JAK2VF mice treated with RUX were fixed in 4% paraformaldehyde for 24 h and then incubated in 30% ethanol for 30 min and 50% ethanol for 24 h. Organs were embedded in paraffin and paraffin sections were cut on a rotary microtome (Microm HM 355S, Thermo Fisher Scientific), mounted on microscope slides (Thermo Fisher Scientific) and air-dried in an oven at 37 °C overnight. Tissue section slides were then processed automatically for H&E staining (Leica AutoStainer XL, Leica Biosystems, Wetzlar, Germany). Images were acquired at  $\times 10$  magnification on an AxioImager A.2 (Carl Zeiss Microscopy, Jena, Germany). Images were processed using the ImageJ software (NIH, Bethesda, MD, USA).

### Experimental animals

All mice were housed under pathogen-free conditions in the accredited Animal Research facility of the Otto von Guericke University Medical Faculty, Magdeburg, or the University Hospital Jena. Animals were maintained in groups in single-ventilated type II long IVC-cages. Room temperature was 22 °C  $\pm$  2 °C and humidity was maintained at 55%  $\pm$  10%. Mice were kept in rooms with light/dark cycle (6am–8pm light, 8pm–6am dark, including a twilight phase in between). All animal experiments have been approved by the respective ethics committees for animal welfare either at the Landesverwaltungsamt Saxony-Anhalt, Halle (State Administration Office Saxony-Anhalt) or at the Landesamt für Verbraucherschutz, Abteilung Gesundheitlicher und technischer Verbraucherschutz, Referat Verbraucherschutz und Veterinärangelegenheiten (Thuringian State Administration Office), Bad Langensalza, Thuringia, Germany. Conventional *Ybx1* knockout mice have been generated as previously described<sup>29</sup>. Mice harbouring a ‘floxed’ (flanked with *loxP* sites) allele of *Ybx1* have been generated at Taconic-Artemis in a C57BL/6 background. Conditional *Jak2<sup>V617F</sup>* knock-in mice have been described previously<sup>30</sup>. In pre-clinical patient-derived xenograft mouse models, paired samples of patient cells were investigated for response to drug treatment versus diluent control. Therefore, no randomization was necessary. Likewise, mouse cells that were either genetically modified or pharmacologically treated were injected at equal distribution into recipient mice. Due to the analysis in paired samples, with pharmacologic therapy or diluent control, no blinding was necessary and possible at the stage of cell transplantation or drug treatment. Specification of sex and gender for the different mouse strains: *Ybx1<sup>+/+</sup>* or *Ybx1<sup>-/-</sup>* donor mice, females and males were used, age 6–8 weeks; *Ybx<sup>+/+</sup> Jak2<sup>VF</sup>* Mx1<sup>+</sup> or *Ybx<sup>-/-</sup> Jak2<sup>VF</sup>* Mx1 donor mice, females and males were used, age 6–8 weeks old; C57BL/6j (CD45.2) recipients, only females were used, age 6–8 weeks; Ly5.1 (CD45.1) recipients, only females were used, age 6–8 weeks; CD45.1/2 competitors, males and females were used (female competitors were paired with female donors and male competitors were paired with male donors), age 6–8 weeks; NSGS recipients, only females were used, age 6–8 weeks. NSGW41 mice were generated and maintained as previously described<sup>31</sup>.

### Haematopoietic progenitor cell assays

**Colony formation assay.** For investigation of colony formation in methylcellulose, LSK (Lin<sup>-</sup> Sca1<sup>+</sup> KIT<sup>+</sup>) cells were sorted from bone marrow of the respective donor mice as previously described.  $1 \times 10^3$  cells were seeded in MethoCult M3434 (Stem Cell Technologies), respectively. Colony numbers were counted on day 8 after plating as previously described<sup>32</sup>.

**Spleen colony formation assays (CFU-S12).** Bone marrow cells were collected from donor mice and  $1 \times 10^2$  LSK cells were FACS sorted and injected via tail vein into lethally irradiated (12 Gy TBI) C57BL/6 recipient mice. At day 12 post-injection, spleens from recipient mice were

harvested and stained with Bouin’s fixative solution (Sigma-Aldrich), and colonies were counted as previously described<sup>33</sup>.

### Transplantation assays and in vivo treatment

For competitive repopulation assays  $2 \times 10^6$  bone marrow (BM) cells (for *Jak2<sup>WT</sup>*) or  $5 \times 10^4$  sorted LSK cells (for *Jak2<sup>VF</sup>*) of 6–8-week-old *Ybx1<sup>-/-</sup>* or *Ybx1<sup>+/+</sup>* (CD45.2) littermates and  $2 \times 10^6$  (CD45.1/2) competitor cells (derived from intercrossing CD45.1 animals with CD45.2 animals purchased from Charles River) were transplanted via lateral tail vein injection into lethally irradiated (12 Gy, single dose) 6–8-week-old Ly5.1 mice (Jackson Laboratories, Bar Harbour, ME). For serial transplantation experiments whole BM of primary recipient mice was harvested and  $2 \times 10^6$  whole BMCs were injected into lethally irradiated secondary recipients. The JAK1/2 inhibitor ruxolitinib was purchased at Selleckchem (S1378) and formulated for administration by oral gavage as previously described<sup>34</sup>. Mice received ruxolitinib (90 mg per kg body weight) or vehicle control by oral gavage twice a day. For engrafting of JAK2-mutated human cells, HEL cells were either infected with lentiviral particles for transduction of the respective shRNAs (shNT or shYBX1) or incubated for 24 h with inhibitors as indicated.  $1 \times 10^6$  viable cells were injected in each irradiated (2 Gy) recipient NSGS mouse via lateral tail vein injection. Engraftment and expansion of human cells was monitored weekly by the presence of hCD45-positive cells in the peripheral blood. For patient derived xenograft experiments (PDX) we used an improved model for human stem cell (HSC) transplantation and analysis that has been developed from immune-deficient mouse strains containing *Kit* mutations (NSGW41)<sup>31</sup>. These mice can be engrafted without prior conditioning and therefore maintain an intact niche and microenvironment. Primary bone marrow samples were acquired during routine biopsies and cells were isolated by Ficoll gradient centrifugation followed by depletion of CD3 positive cells.  $1.8 \times 10^6$  human stem- and progenitor cells (HSPCs) were engrafted (pairwise) per animal. Mice were followed for 4 weeks and peripheral blood chimerism of human CD45 positive cells was measured by flow cytometry. Between weeks 4 and 20 all animals were treated for 5 d every 4 weeks with either ruxolitinib (90 mg/kg twice a day per gavage) or the combination of ruxolitinib with the MEK/ERK inhibitor trametinib (1 mg/kg daily per gavage).

### Quantification of JAK2VF mutant cells by pyrosequencing

In order to assess for the relative abundance of JAK2-mutated cells within the patient derived xenograft (PDX) model, we sorted human CD45 positive cells from the bone marrow at week 20 and performed pyrosequencing for the JAK2<sup>VF</sup> mutation. DNA isolation and whole-genome amplification were carried out on FACS-sorted hCD45 positive cells using the REPLI-g Single Cell Kit (Qiagen, Hilden, Germany) according to the manufacturer’s instructions. Amplicons were generated using AmpliTaq Gold DNA Polymerase (Thermo Fisher Scientific, Waltham, MA, USA; biotinylated forward primer: GAAGCAGCAAGTATGATGAGCA; reverse primer: TGCTCTGAGAAAGGCATTAGAA) according to standard protocols. Samples were then analysed by pyrosequencing (PyroMark Q96 ID, Qiagen, Hilden, Germany; sequencing primer: TCTCGTCTC-CACAGA) to assess for the mutational status of the JAK2<sup>V617F</sup> variant of the individual subpopulations.

### Rescue of shRNA-inactivated endogenous YBX1 with exogenous enforced expression of Mcl-1

Ba/F3 cells expressing EpoR (MSCV-EpoR-Neo) and JAK2VF-GFP (MSCV-Jak2VF-GFP) were infected with retrovirus expressing empty vector (MSCV-Puro) or Mcl-1 (MSCV-Mcl-1-Puro). Knockdown of *Ybx1* was performed as indicated.

### Immunoprecipitation and immunoblotting

For western blot analysis samples were collected in freshly prepared RIPA buffer containing 1 $\times$  Protease Inhibitor cocktail (Roche) and 1 $\times$

# Article

PhosphoSTOP (Roche). For immunoprecipitation samples were collected in freshly prepared IP buffer (150 mM NaCl, 50 mM Tris (pH 7.5), 5% glycerol, 1% IGPAL-CA-630, protease inhibitors (EDTA-free), 1 mM MgCl<sub>2</sub>, Benzonase, 1× Protease Inhibitor cocktail and 1× PhosphoSTOP). In case of JAK2–YBX1 interaction analysis, Ba/F3 EpoR and wild-type *Jak2* or *Jak2*<sup>V617F</sup> cells were washed twice with PBS and starved for 4 h in serum-reduced (0.5%) medium at a density of  $1 \times 10^6$ /ml. TrueBlot Anti-Rabbit Ig IP Beads Kit (Rockland Immunochemicals, Gilbertsville, PA, USA) was used following the manufacturer's instruction. The following antibodies were purchased from Cell Signaling (Danvers, MA, USA) and used at a 1:1,000 dilution: GFP (2555S), MNK1 (2195), p-AKT (9271), AKT (9272), p-p44/42 MAPK (9106), p44/42 MAPK (9102 and 4695), cRAF (9422), p-JAK2 (3771), JAK2 (3230), pSTAT3 (9134), STAT3 (9139), BIM (2933) and BCL-XL (2764). GAPDH antibody (H86504M, 1:5,000) was purchased from Meridian Life Sciences (Memphis, TN, USA), p-STAT5 antibody (05–495, 1:1,000) was purchased from Millipore (Darmstadt, Germany) and STAT5 (sc-1081, 1:100) antibody from Santa Cruz Biotechnologies (Dallas, TX, USA). MCL-1 antibody (600-401-394, 1:1,000) was received from Rockland Immunochemicals (Limerick, PA, USA), Vinculin was from Sigma (V9131, 1:5,000) and YBX1 antibody (ab76149, 1:1,000) was from Abcam (Cambridge, UK). All the uncropped western blot images were provided as source data in the supplement data figure.

## Flow cytometry

For immunophenotype analysis, peripheral blood cells, bone marrow or spleen cells were resuspended in PBS/1% FBS after erythrocyte lysis (PharmLyse, BD Pharmingen). Unless otherwise stated, the following antibodies were used: sorting and analysis of LSK-cells or Sca-1<sup>+</sup> cells were performed as previously described<sup>35,36</sup>. Biotinylated antibodies against Gr-1 (RB6-8C5), B220 (RA3-6B2), CD19 (6D5), CD3 (145-2C11), CD4 (GK1.5), CD8 (53-6.7), TER119 and IL7Ra (A7R34) (all Biolegend, San Diego, CA, USA) were used for lineage staining in a 1:500 dilution. APC-Cy7- or BV421-labelled streptavidin antibodies (Biolegend) were used for secondary staining together with an APC-anti-KIT (clone 2B8) and a FITC- or PE-anti-Sca-1 antibody (clone E13-161.7). All surface marker antibodies were used in a 1:100 dilution. Cells were sorted on a BD FACSAria III, analysis of the cells was performed using a FACSCantoII (Becton Dickinson) cytometer and FlowJo software (Treestar, Ashland, OR, USA). Fix & Perm Kit (Life Technologies) was used for intracellular staining according to the manufacturer's protocol. The following antibodies were used: MNK1 antibody (Thermo Fisher Scientific, 711542; 1:100), p-p44/42 (ERK1/2)-Alexa Fluor 647 (Cell Signaling, 13148S, 1:50).

## Immunofluorescence analysis (JAK2–YBX1 co-localization)

$2 \times 10^4$  cells were washed and seeded onto adhesion slides (Marienfeld). Attached cells were fixed in PBS/2% PFA/0.01% glutaraldehyde for 15 min on ice followed by permeabilization for 10 min with PBS/0.02% Triton X-100 at room temperature. After blocking for 30 min with PBS/1% BSA/0.1% Tween 20, YBX1 antibody (Abcam ab76149, 1:250) was incubated in blocking solution for 1 h. The samples were washed 5 times, 5 min per washing step, with PBS and then incubated with Alexa Fluor 488 or 568 donkey anti-rabbit antibody (Life Technologies A21206, A11036 at 1:200 dilution) for 1 h. After additional washing, JAK2 antibody labelled with Cy3 (BIOSUSA bs-0908R-Cy3, 1:50) was incubated in blocking solution for 1 h. The samples were then washed, incubated with DAPI (Thermo Scientific #R37606) for 10 min and mounted using ProTaq Mount Fluor (Quartett, 401603095). Samples were analysed using a confocal microscope (Leica SP8 or Zeiss LSM-780) and ImageJ for quantification.

## Generation of YBX1 phosphorylation mutants

Phosphorylation mutants mimicking hyperphosphorylation or de-phosphorylation of YBX1 were generated by site-directed mutagenesis (as previously described<sup>37</sup>) at amino acid residues that

were (i) highly conserved and (ii) differentially phosphorylated in the absence or presence of mutant JAK2 kinase. These aspects applied to the mouse serine residues S30, S34, S172 and S174. In detail the following mutants were generated by site directed mutagenesis using a retroviral MSCV-IRES-GFP backbone: (1) MIG-mYbx1-S30A/S34A; (2) MIG-mYbx1-S30A; (3) MIG-mYbx1-S34A; (4) MIG-mYbx1-S30D/S34D; (5) MIG-mYbx1-S30D; (6) MIG-mYbx1-S34D and (7) MIG-mYbx1-S172A/S174A. Constructs were expressed in mouse Ba/F3-JAK2VF cells. In brief, cells were infected by co-localization of virus supernatant (containing the respective constructs as indicated above) with Ba/F3-JAK2-V617F (VF) cells on RetroNectin-coated plates. Infection has been repeated after 24 h and GFP-positive cells were sorted to ensure expression of the mutants in a homogeneous population.

## Statistical analysis

For survival analysis, Kaplan–Meier curves were plotted using GraphPad Prism version 6.0h (GraphPad Software, San Diego, CA). Differences between survival distributions were analysed using the log-rank test. Statistical analyses were performed using Student's *t*-test (normal distribution) or Mann–Whitney *U* test (when normal distribution was not given).  $P < 0.05$  was considered statistically significant.

## Reporting summary

Further information on research design is available in the Nature Research Reporting Summary linked to this paper.

## Data availability

The MS raw data files and Maxquant output files reported in this manuscript are available at ProteomeXchange Consortium with the data identifier PXD006921. RNA-seq data have been deposited in the Gene expression Omnibus database with accession number GSE123417. ChIP-Seq data has been deposited to the Gene expression Omnibus database with the accession code GSE154025 for mouse and GSE146717 for human. All other data supporting the findings of this study are available from corresponding authors upon reasonable request. Source data are provided with this paper.

- Humphrey, S. J., Karayel, O., James, D. E. & Mann, M. High-throughput and high-sensitivity phosphoproteomics with the EasyPhos platform. *Nat. Protocols* **13**, 1897–1916 (2018).
- Kulak, N. A., Pichler, G., Paron, I., Nagaraj, N. & Mann, M. Minimal, encapsulated proteomic-sample processing applied to copy-number estimation in eukaryotic cells. *Nat. Methods* **11**, 319–324 (2014).
- Cox, J. & Mann, M. MaxQuant enables high peptide identification rates, individualized p.p.b.-range mass accuracies and proteome-wide protein quantification. *Nat. Biotechnol.* **26**, 1367–1372 (2008).
- Tyanova, S. & Cox, J. Perseus: a bioinformatics platform for integrative analysis of proteomics data in cancer research. *Methods Mol. Biol.* **1711**, 133–148 (2018).
- Dobin, A. et al. STAR: ultrafast universal RNA-seq aligner. *Bioinformatics* **29**, 15–21 (2013).
- Liao, Y., Smyth, G. K. & Shi, W. featureCounts: an efficient general purpose program for assigning sequence reads to genomic features. *Bioinformatics* **30**, 923–930 (2014).
- Ritchie, M. E. et al. limma powers differential expression analyses for RNA-sequencing and microarray studies. *Nucleic Acids Res.* **43**, e47 (2015).
- Romero, J. P. et al. EventPointer: an effective identification of alternative splicing events using junction arrays. *BMC Genomics* **17**, 467 (2016).
- Schnöder, T. M. et al. Cell autonomous expression of CXCL10 in JAK2V617F-mutated MPN. *J. Cancer Res. Clin. Oncol.* **143**, 807–820 (2017).
- Webb, C. H. & Hertel, K. J. Preparation of splicing competent nuclear extracts. *Methods Mol. Biol.* **1126**, 117–121 (2014).
- Uckelmann, H. J. et al. Therapeutic targeting of preleukemia cells in a mouse model of *NPM1* mutant acute myeloid leukemia. *Science* **367**, 586–590 (2020).
- Lu, Z. H., Books, J. T. & Ley, T. J. YB-1 is important for late-stage embryonic development, optimal cellular stress responses, and the prevention of premature senescence. *Mol. Cell. Biol.* **25**, 4625–4637 (2005).
- Mullally, A. et al. Physiological Jak2V617F expression causes a lethal myeloproliferative neoplasm with differential effects on hematopoietic stem and progenitor cells. *Cancer Cell* **17**, 584–596 (2010).
- Cosgun, K. N. et al. Kit regulates HSC engraftment across the human-mouse species barrier. *Cell Stem Cell* **15**, 227–238 (2014).
- Schnöder, T. M. et al. Epo-induced erythroid maturation is dependent on Plcγ1 signaling. *Cell Death Differ.* **22**, 974–985 (2015).
- Till, J. E. & McCulloch, E. A. A direct measurement of the radiation sensitivity of normal mouse bone marrow cells. *Radiat. Res.* **14**, 213–222 (1961).



34. Quintás-Cardama, A. et al. Preclinical characterization of the selective JAK1/2 inhibitor INCB018424: therapeutic implications for the treatment of myeloproliferative neoplasms. *Blood* **115**, 3109–3117 (2010).
35. Heidel, F. H. et al. The cell fate determinant Lgl1 influences HSC fitness and prognosis in AML. *J. Exp. Med.* **210**, 15–22 (2013).
36. Heidel, F. H. et al. Genetic and pharmacologic inhibition of  $\beta$ -catenin targets imatinib-resistant leukemia stem cells in CML. *Cell Stem Cell* **10**, 412–424 (2012).
37. Arriba-Tutusaus, P. et al. Impact of FLT3-ITD location on sensitivity to TKI-therapy in vitro and in vivo. *Leukemia* **30**, 1220–1225 (2016).

**Acknowledgements** We thank A. Fenske (Central Animal Facility, OvGU Magdeburg) and M. van der Wall (Central Animal Facility, University Hospital Jena) for support with animal care; the Animal Facility of the Leibniz Institute on Aging Jena for providing NSGW41 animals; R. Hartig (FACS Core Facility, Medical Faculty, and CRC854, OvGU Magdeburg) and K. Schubert (FACS Core Facility, Leibniz-Institute on Aging, Jena) for support with cell sorting, M. Milsom (DKFZ, Heidelberg) for providing constructs; S. Frey, A. Sammt and C. Kathner-Schaffert for technical assistance; K. Mayr, I. Paron and G. Sowa for their assistance and support in the mass spectrometry analysis (MPI Biochemistry); M. Driessen for RNA sequencing and S.-H. Yu for CHIP sequencing analysis (Bioinformatics Core Facility, MPI Biochemistry); and Th. Fischer (Magdeburg), K.L. Rudolph (Jena) and C. Müller-Tidow (Heidelberg) for helpful comments and discussions.

**Author contributions** Conception and design: A.K.J., T.M.S., S.W.L., F.H.H. Development of methodology: A.K.J., T.M.S., C.H., M.M., F.H.H. Acquisition of data (provided animals, acquired and managed patients, provided facilities etc.): T.M.S., A.K.J., G.K., C.H., F. Perner, J.M., B.E.-S., N.S., T.E., A.M., B.I., P.R.M., S.W.L., M.M., F.H.H. Analysis and interpretation of data (e.g., computational analysis, statistical analysis): A.K.J., C.H., T.M.S., A.M., N.H., S.J., A.S., F.E., M.U., T.E., C.A.H., A.H., L.B., S.W.L., F.H. Writing, review and/or revision of the manuscript: A.K.J., T.M.S., F. Palandri, F. Perner, L.B., S.W.L., P.J.J., R.Z., A.M., P.R.M., C.W., B.I., M.M., F.H.H..

Administrative, technical or material support: A.K.J., C.H., T.M.S., J.M., B.E.-S., F. Palandri, G.K., R.A., S.B., N.S., S.J., I.C., A.M., S.R., C.W., M.M., A.H., B.I., P.R.M. Study supervision: M.M., F.H.H. This work was supported by grants of the German Research Council (DFG; HE6233/4-1 and 4-2 to F.H.H.), by the DFG-Collaborative Research Center (CRC854/2) to P.R.M. (Project A1), B.I. (Project B26N) and F.H.H. (Project A20) and by the Thuringian state program ProExzellenz (RegenerAging-FSU-I-03/14) of the Thuringian Ministry for Economics, Science and Digital Society (TMWWDG; to F.H.H.). A.K.J. and M.M. were supported by the Max Planck Society for the Advancement of Science and by the German Research Foundation (DFG/Gottfried Wilhelm Leibniz Prize). P.J.J. by DFG (SFB1335) and F. Perner was supported by a DFG fellowship grant (PE-3217/1-1). G.K. was supported by ERC starting grant 635617 and the DFG (SFB-TR128-A1). C.W. was supported by FOR2033-A03, TRR127-A5, WA2837/6-1 and WA2837/7-1. R.Z. was supported by the Deutsche Krebshilfe grant #70113473 and the ERC Consolidator grant (681012 GvHDCure). S.W.L. has received research funding support from the Australian National Health and Medical Research Council (NHMRC).

**Competing interests** F.H.H. has served as an advisory board member for and received research funding from Novartis, Celgene and CTI. S.W.L. has served on an advisory board for Novartis Australia. A.H. received research support by Novartis, BMS, Pfizer, Incyte. A.M. has received honoraria from Blueprint Medicines, Roche and Incyte and receives research support from Janssen and Actuate Therapeutics. No potential conflicts of interest were disclosed by the other authors.

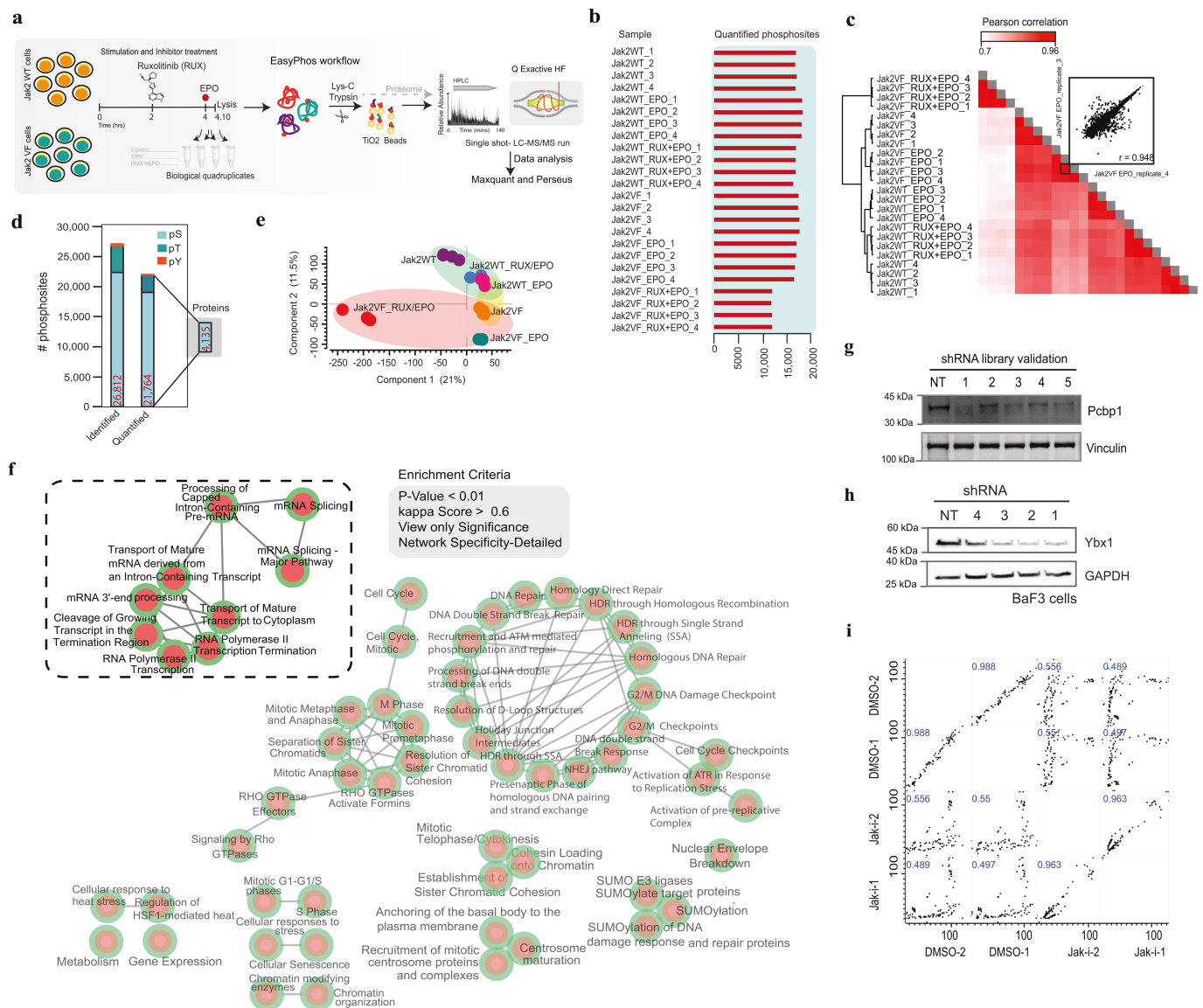
#### Additional information

**Supplementary information** is available for this paper at <https://doi.org/10.1038/s41586-020-2968-3>.

**Correspondence and requests for materials** should be addressed to M.M. or F.H.H.

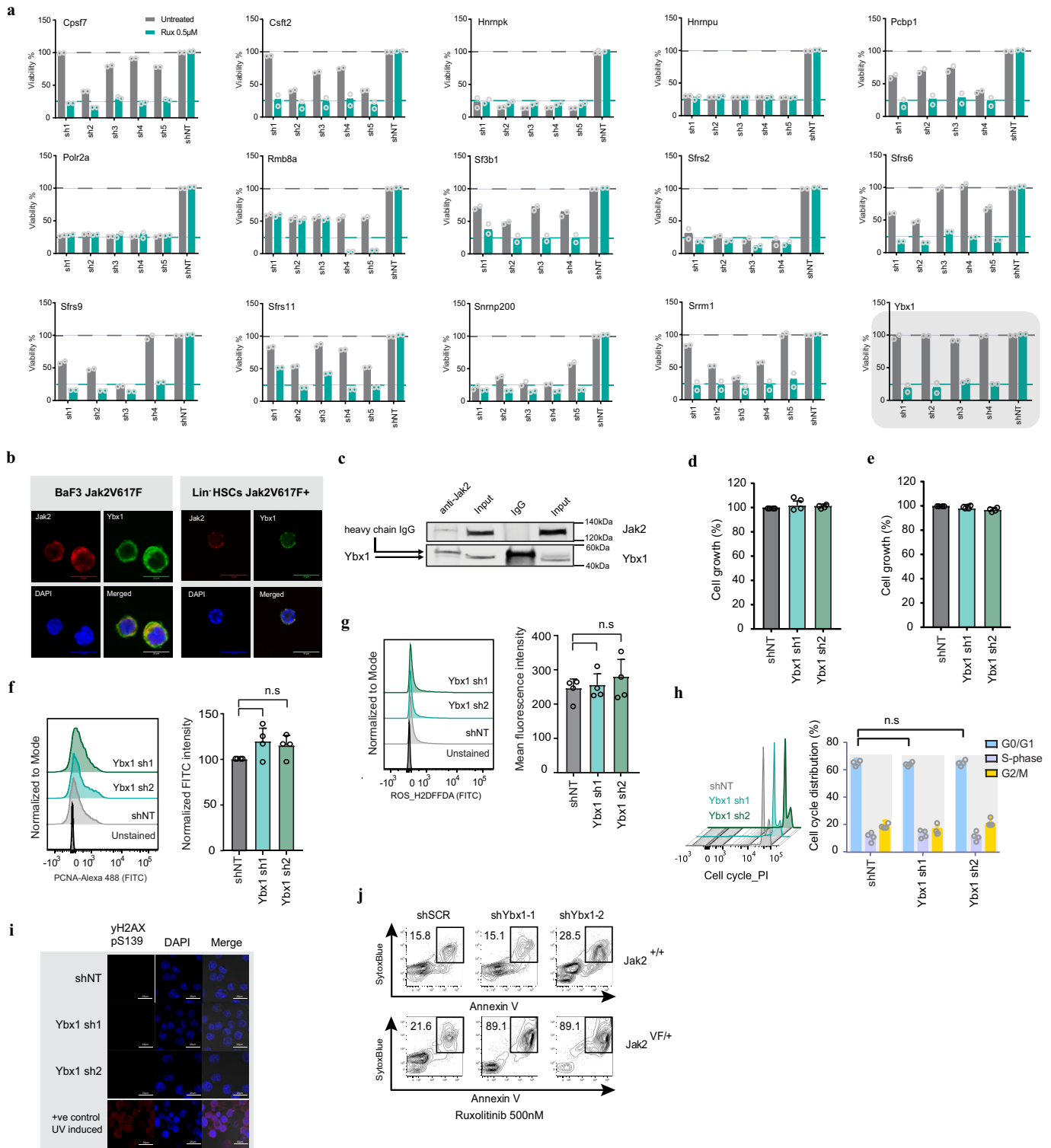
**Peer review information** *Nature* thanks Fabienne Meier-Abt, Michael Yaffe and the other, anonymous, reviewer(s) for their contribution to the peer review of this work.

**Reprints and permissions information** is available at <http://www.nature.com/reprints>.



**Extended Data Fig. 1 | Phosphoproteomic analysis uncovers differential regulation of splicing factors in *Jak2*-mutated cells.** **a**, Schematic of the phosphoproteome workflow. Following sample collection, phosphopeptides were enriched using EasyPhos workflow<sup>8</sup> and analysed in single-run LC-MS/MS. Data were analysed in Maxquant and Perseus. **b**, Quantified phosphosite depth per sample. Samples were measured as biological quadruplicates. **c**, Heatmap of sample correlation matrix of all measured samples (in **b**) based on Pearson correlation values. The reproducibility between the phosphoproteome sample is highlighted. **d**, Summary of identified and quantified class-I phosphosites (localization probability of >0.75) corresponding to number of proteins of this

experiment. **e**, Principal component analysis of the samples. **f**, Network map of significantly enriched GO terms ( $P$  value < 0.05) of differentially phosphorylated proteins in *JAK2V617F*. Phosphorylated proteins significantly regulated in *Jak2V617F* were subsequently used as an input for *Cytoscape* to obtain the network. The highlighted sub-network was obtained with  $P$  value < 0.01 and kappa score > 0.6. Two-sided hypergeometric test,  $P$  value correction - Bonferroni stepdown (**g**, **h**), western blot validation of shRNA library targets. **g**, *Pcbp1* protein and **h**, *YBX1* protein in mouse *JAK2VF* cells.  $n = 3$  with comparable results. **i**, Pearson correlation profile of the independent shRNA experiments.



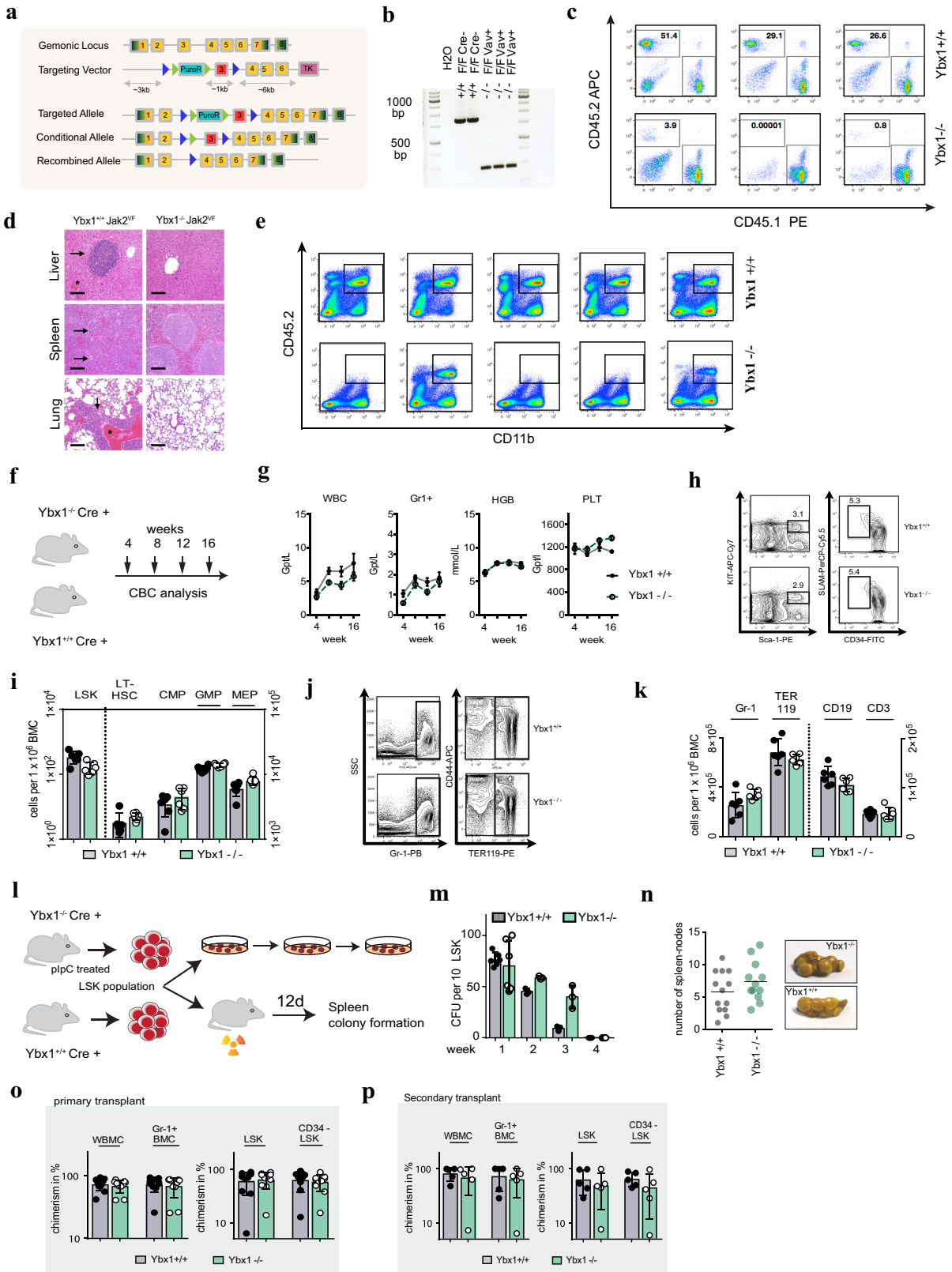
**Extended Data Fig. 2** | See next page for caption.

# Article

**Extended Data Fig. 2 | Functional consequences of YBX1 depletion in *Jak2*-mutated cells.** **a**, In vitro shRNA validation of selected top 15 targets essential for JAK2VF cell survival and growth in the presence (green) and absence (grey) of JAK inhibitor (RUX, 0.5  $\mu$ M) measured by proliferation assays (16 technical replicates measured in 2 plates independently, mean). **b**, Immunofluorescence analysis of YBX1 and JAK2 localization in JAKVF positive Ba/F3 cells (left) and mouse JAK2<sup>VF</sup> positive stem- and progenitor cells (lineage-negative cells) (right panel) (representative image of  $n = 3$ ). **c**, Immunoprecipitation of JAK2 receptor from mouse JAK2VF cells showing binding of YBX1 to mutated JAK2 receptor ( $n = 3$  with similar results). **d**, **e**, Percentages of cell growth in JAK2WT (**d**) and JAK2VF cells (**e**) following lentiviral infection with shRNAs targeting *Ybx1* or non-targeting control (shNT) measured by MTS assay. **f**, Representative

histogram and bar plot showing ROS levels measured in JAK2VF cells with shRNAs targeting *Ybx1* or control. **g**, Representative histogram and bar plot showing proliferative marker PCNA levels in JAK2VF cells with shRNAs targeting *Ybx1* or control. **h**, Cell cycle analysis after YBX1 inactivation in JAK2VF cells. **d-h**,  $n = 4$  independent experiments, mean  $\pm$  s.d., two-tailed *t*-test with equal variance. **i**, Representative confocal images of DNA damage marker  $\gamma$ H2AX pS139 in JAK2VF cells with shRNAs targeting *Ybx1* or non-targeting control. Cells exposed to UV light for 20 min were used as positive controls ( $n = 4$  independent experiments). **j**, FACS plots showing percentage of apoptotic cells in *Jak2*<sup>+/+</sup> and *Jak2*<sup>VF/+</sup> mouse BM cells after JAK inhibitor treatment (RUX, 0.5  $\mu$ M) after lentiviral knockdown of *Ybx1* (sh1 and sh2) compared to non-targeting control (shNT).





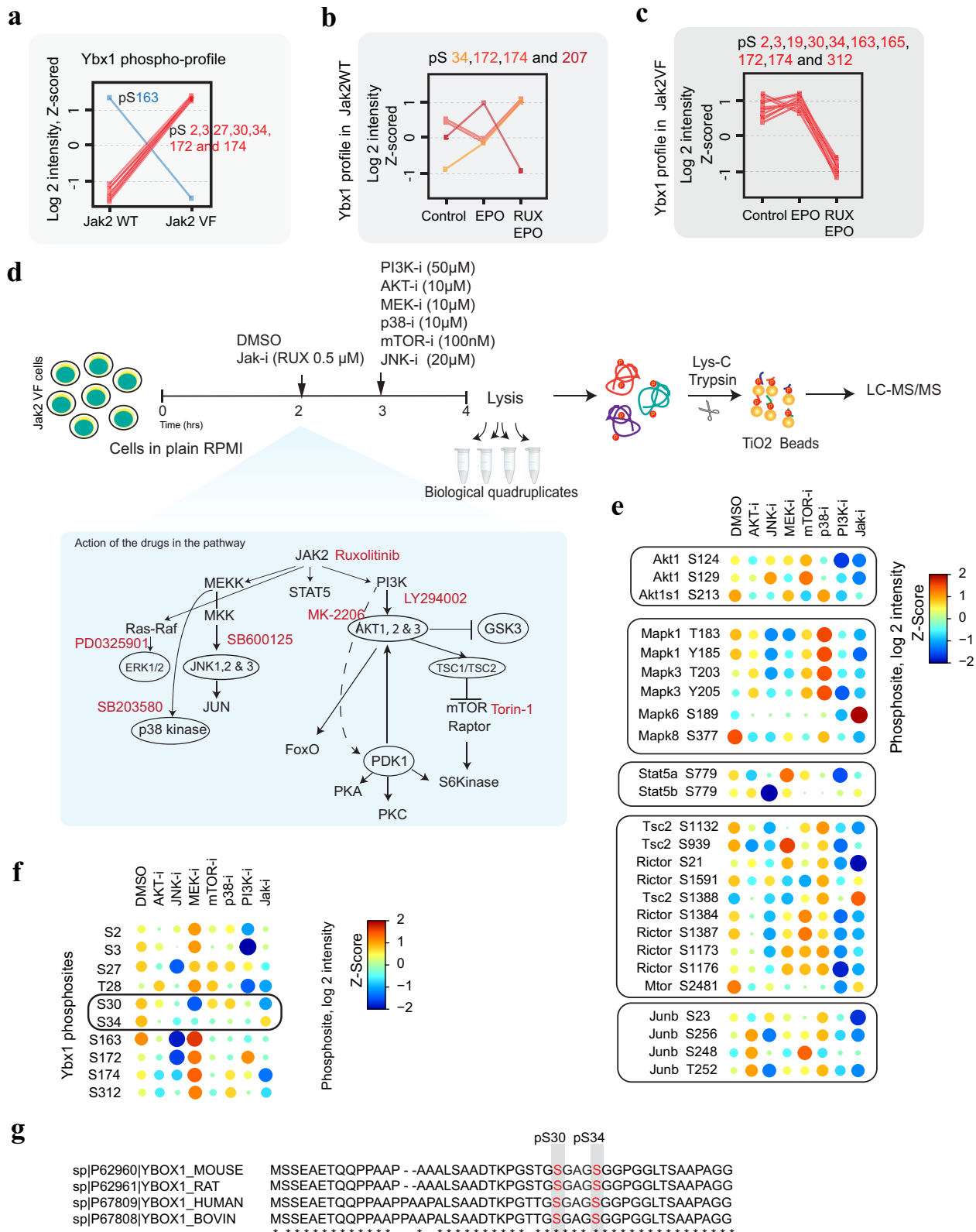
Extended Data Fig. 3 | See next page for caption.

# Article

## Extended Data Fig. 3 | Functional consequences of *Ybx1* deletion in vivo.

**a**, Schematic representation of the wild-type *Ybx1* allele (Genomic Locus), the targeting vector (Targeting Vector), the desired targeted allele (Targeted Allele), the desired conditional allele flanked by LoxP sequences (Conditional Allele) and the null recombined allele (Recombined Allele) after Cre-mediated recombination of the conditional allele. Triangles indicate loxP sequences. **b**, Excision control by genomic PCR on whole bone marrow cells at week 16 following genetic inactivation of *Ybx1* in conditional knockout mice. Representative micrograph of  $n = 5$  animals from a total of  $n = 9$  controls (+/+) and  $n = 9$  knockout (-/-) replicates. **c**, Schematic as in Fig. 2j. FACS plots showing percentage of  $Jak2^{V617F}$  (CD45.2) cells of  $Ybx1^{+/+}$  or  $Ybx1^{-/-}$  recipients. **d**, Histology of liver, spleen and lung of  $Jak2^{V617F}$ - $Ybx1^{+/+}$  and  $Jak2^{V617F}$ - $Ybx1^{-/-}$  recipient mice at week 20 after BMT. Representative micrographs of  $n = 9$  individual mouse replicates. Haematoxylin and eosin stain (H&E) at  $\times 10$  magnification. Focal leukocyte infiltration (arrows) and haemorrhage (stars) of liver, spleen and lung, respectively. Scale bar: 200  $\mu\text{m}$ . **e**, Peripheral blood chimerism of lethally irradiated (12 Gy) recipient mice. FACS plots showing abundance of CD45.2 myeloid cells in  $Jak2^{V617F}$ - $Ybx1^{+/+}$  and  $Jak2^{V617F}$ - $Ybx1^{-/-}$  recipient mice at week 20 after BMT. **f**, Design for assessment of steady state haematopoiesis. **g**, White blood count (WBC), Gr-1 positive cells (Gr1<sup>+</sup>), haemoglobin (HGB) and platelets (PLT) following genetic inactivation of *Ybx1* ( $Ybx1^{-/-}$  mice,  $n = 10$ ) compared to  $Ybx1^{+/+}$  controls ( $n = 10$ ). Data represented as mean  $\pm$  s.e.m. **h**, FACS plots showing comparable percentages of LSK cells and

HSCs (SLAMF<sup>+</sup>CD34<sup>-</sup>L<sup>+</sup>S<sup>+</sup>K<sup>+</sup> cells) following genetic inactivation of *Ybx1* in conditional knockout mice (compared to wildtype littermate controls). **i**, stem- and progenitor cell numbers per  $1 \times 10^6$  whole bone marrow cells at week 16 after genetic inactivation of *Ybx1* ( $n = 6$ ; mean  $\pm$  s.d.). **j**, FACS plot showing comparable abundance of mature myeloid and erythroid cells following genetic deletion of *Ybx1*. **k**, Total numbers of mature blood cells of the myeloid (Gr1<sup>+</sup>), erythroid (TER119<sup>+</sup>), B-lymphoid (CD19) and T-lymphoid (CD3) lineages at week 16 after genetic inactivation of *Ybx1* ( $n = 6$ ; mean  $\pm$  s.d.). **l**, Experimental protocol for investigation of haematopoietic progenitor cell function. **m**, Colony numbers of  $Ybx1^{+/+}$  versus  $Ybx1^{-/-}$  mouse stem/progenitor cells. Colonies were counted at day 8 after plating (each sample plated in duplicate,  $n = 3$  independent experiments, mean  $\pm$  s.d.). **n**, Spleen colony numbers counted on day 12 after injection of  $Ybx1^{+/+}$  or  $Ybx1^{-/-}$  LSK cells into lethally irradiated (12Gy) recipient mice (CFU-S12) ( $n = 12$   $Ybx1^{+/+}$ ;  $n = 12$   $Ybx1^{-/-}$  independent biological mouse replicates in  $n = 3$  independent cohorts). **o**, BM chimerism of primary recipient mice ( $n = 10$  individual biological replicates) at week 20 after BMT. Whole bone marrow chimerism (WBMC) and chimerism of myeloid cells (Gr1<sup>+</sup> BMC) (left panel). HSPC chimerism (LSK) and HSC chimerism (CD34<sup>+</sup> LSK) (right panel). Data shown as mean  $\pm$  s.d. **p**, BM chimerism of secondary recipient mice ( $n = 5$  individual biological replicates) at week 20 after BMT. Whole BM chimerism (WBMC) and chimerism of myeloid cells (Gr1<sup>+</sup> BMC) (left panel). HSPC chimerism (LSK) and HSC chimerism (CD34<sup>+</sup> LSK) (right panel). Data shown as mean  $\pm$  s.d.



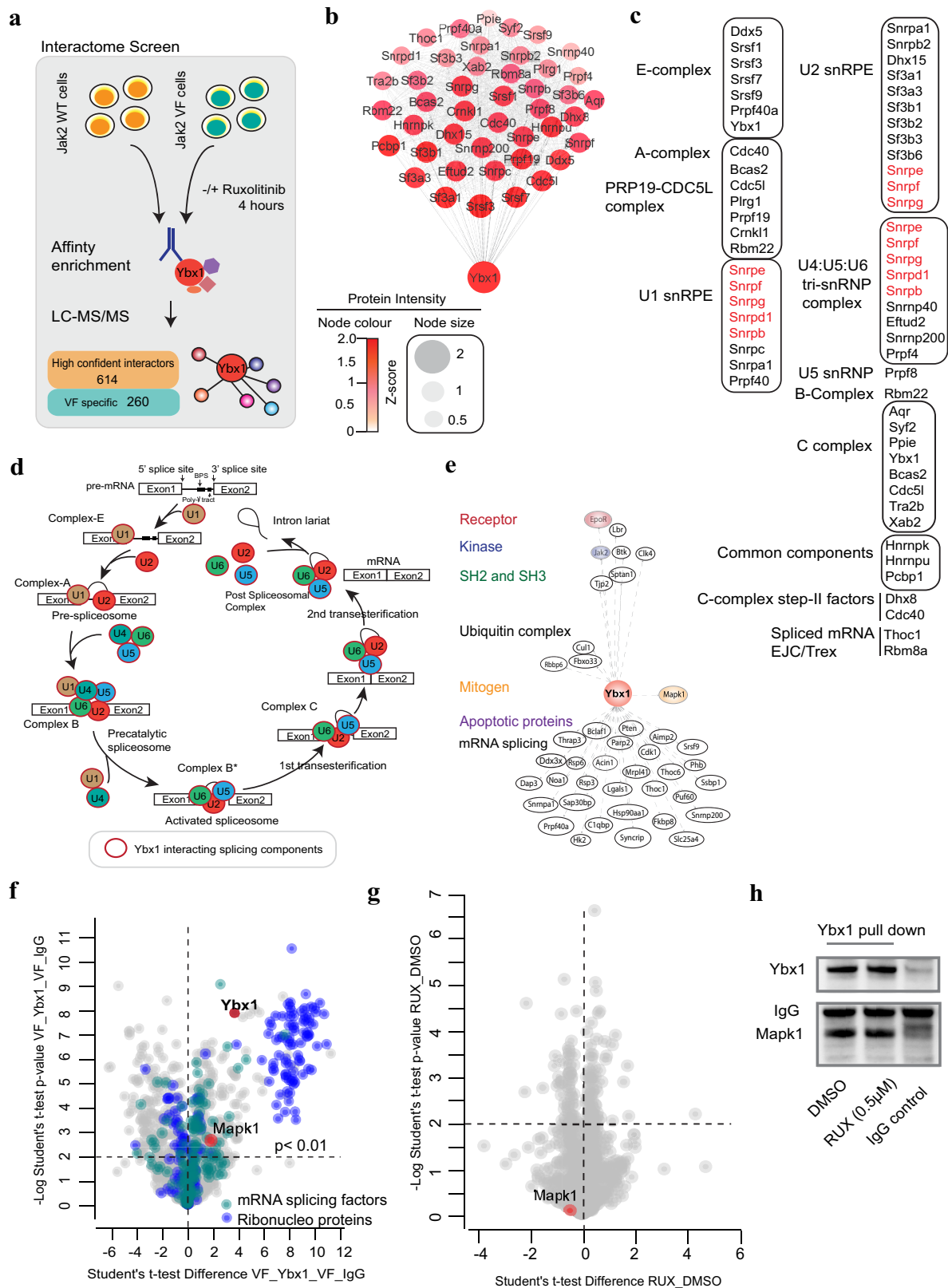
Extended Data Fig. 4 | See next page for caption.

# Article

**Extended Data Fig. 4 | Regulation of YBX1 phosphorylation dynamics in JAK2VF cells.** **a**, Profile plot showing significantly regulated individual phosphorylated residues of YBX1 in JAK2WT and JAK2VF. Each data point is the averaged median of biological quadruplicate and significance was tested using two-sample test. **b**, Profile plot showing individual phosphorylated residues of YBX1 that are significantly regulated in JAK2WT when unstimulated (control) or stimulated with erythropoietin or erythropoietin + JAK inhibitor. **c**, Profile plot showing significantly regulated individual phosphorylated residues of YBX1 in JAK2VF when unstimulated or stimulated with EPO or EPO + JAK inhibitor. **b, c**, Each data point is the averaged median of biological quadruplicate, z-scored ( $\log_2$  phosphosite intensity), and significance was tested using multiple sample test. **d**, Experimental design for phosphoproteome analysis of short-term JAK2 downstream effector kinase

inhibitor treatment in JAK2VF cells.  $n = 4$  per group, phosphopeptides were enriched using EasyPhos workflow and analysed in single-run LC-MS/MS. **e**, Dot plot showing the successful inhibition of respective targets of the corresponding kinase inhibitor used in this study (ANOVA test with permutation-based FDR < 0.01). **f**, Dot plot showing changes in quantified YBX1 phosphosites after various kinase inhibitor treatment (ANOVA test, permutation-based FDR < 0.01). The highlighted YBX1 pS30 phosphosite is the only site highly significantly downregulated upon MEK/ERK inhibitor treatment compared to controls. **e, f**, Size and colour of the dots are proportional to the phosphosite intensity, z-scored ( $\log_2$  intensity). **g**, Amino acid sequence alignment of YBX1 across different species shows that mouse YBX1 Ser30 and Ser34 are conserved.





Extended Data Fig. 5 | See next page for caption.

# Article

**Extended Data Fig. 5 | YBX1 interaction with spliceosome components and validation of YBX1-MAPK1 partnership.** **a**, Study design of mouse YBX1 interactome.  $n = 4$  biological replicates and YBX1 interactome analysed in LC-MS/MS. Using *Perseus*, samples were filtered for a minimum of three valid values in at least one group. In total 614 high confident interactors of YBX1 were identified ( $t$ -test with permutation-based FDR  $< 0.05$ ) with 260 JAK2VF-specific interactors. **b**, Network representation of YBX1 interacting spliceosomal proteins in JAK2VF cells. The size and colour of the node indicates the abundance of the corresponding proteins ( $z$ -scored protein intensity) and the edges are connected by STRING database interactions. **c**, List of significant YBX1-interacting spliceosomal proteins presented according to their spliceosome complex. **d**, Spliceosome proteins interacting with YBX1 participate in spliceosome assembly reaction in a stepwise manner to excise intronic sequences from immature mRNA to form a mature mRNA. **e**, Network

representation of YBX1 interactome (regulated in both JAK2WT and JAK2VF) based on annotation keywords. The keywords are highlighted in colours according to the protein function.  $n = 4$  biological replicates,  $t$ -test with permutation-based FDR  $< 0.05$ . **f**, Scatter plot of YBX1 interactome in JAK2VF vs control. YBX1 interactome is enriched for GO term mRNA splicing factor (green) and Ribonucleoproteins (blue) assessed by Fisher's exact test. Fold enrichment of YBX1 and MAPK1 in JAK2VF cells compared to IgG control plotted against  $-\log_{10}$  Student  $t$ -test  $P$  value. **g**, Scatter plot of YBX1 interactome in DMSO vs JAK inhibitor (RUX 0.5  $\mu$ M, 4 h)-treated JAK2VF cells. Fold enrichment of MAPK1 in DMSO vs JAK inhibitor plotted against  $-\log_{10}$  Student's  $t$ -test  $P$  value. **h**, Immunoprecipitation of YBX1 from mouse JAK2VF cells  $\pm$  RUX, 0.5  $\mu$ M for 4 h and analysed for interaction with MAPK1 by western blot analysis using ERK1/2 antibody. Representative images from  $n = 3$  biological experiments.



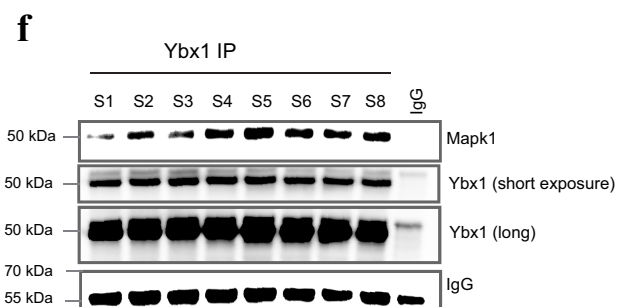
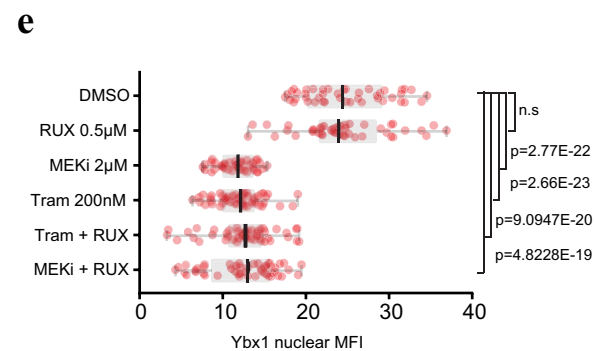
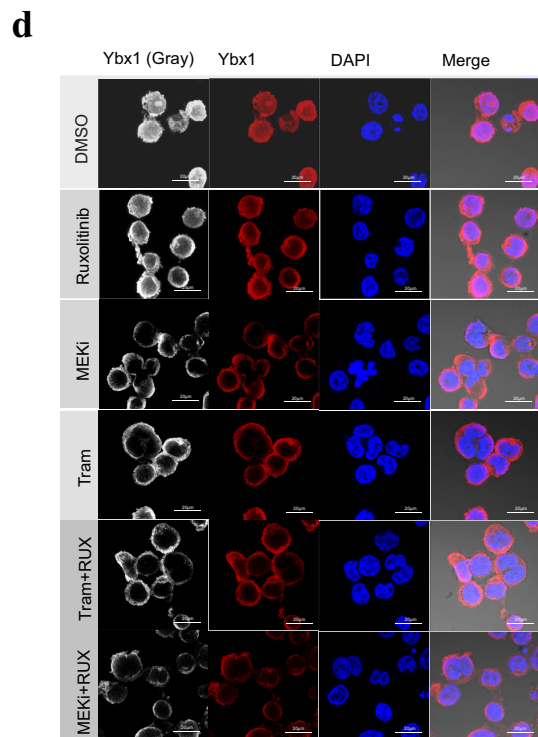
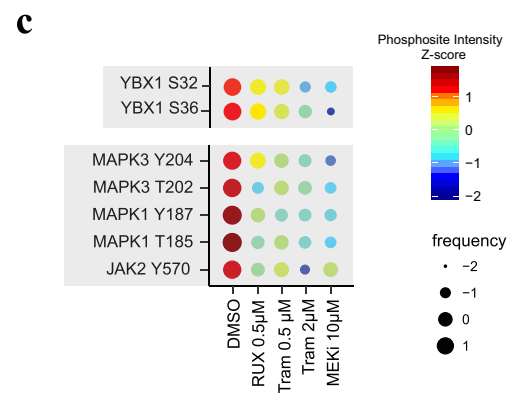
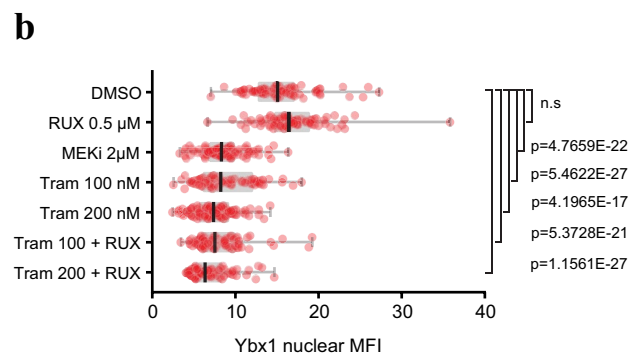
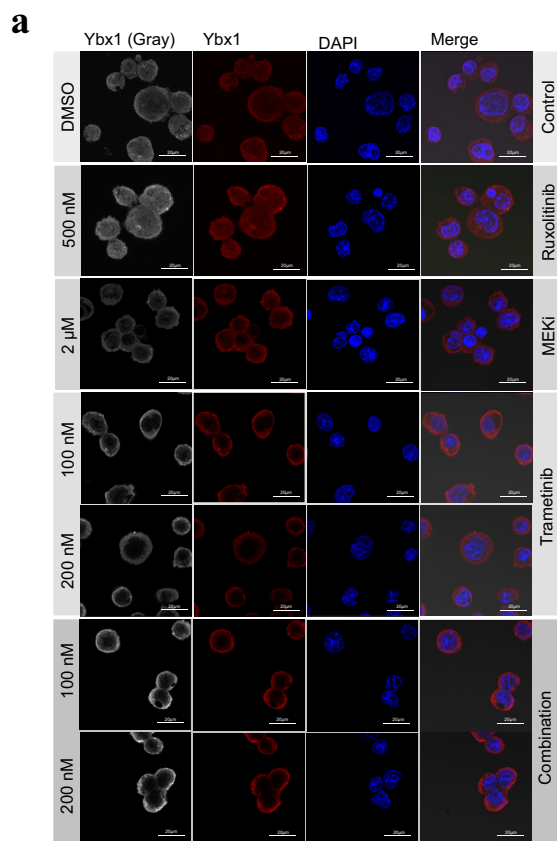
# Article

## Extended Data Fig. 6 | YBX1 phospho-null mutants display impaired

**nuclear localization and increased sensitivity to JAK inhibitor.** **a**, Western blot showing the expression of YBX1 phosphomutants in Ba/F3 JAK2VF cells as indicated. **b**, Confocal images of YBX1 localization (Red) in YBX1 phosphomutants expressing Ba/F3 JAK2VF cells. Cells were counterstained with DAPI and GFP confirms the phosphomutant expression.

**a b**, Representative images from  $n = 3$  biological experiments. **c**, Bar plot showing quantification of nuclear YBX1 expression in YBX1 phosphomutants expressing Ba/F3 JAK2VF cells;  $P$  values were determined by two-tailed  $t$ -test. Control ( $n = 67$ ): min = 15.39; max = 33.01; whisker = [15.39–33.01]; median = [24.74], S1( $n = 70$ ): min = 4.14; max = 9.75; whisker = [4.14–9.75]; median = [7.0053], S2( $n = 64$ ): min = 5.32; max = 14.11; whisker = [5.32–14.11]; median = [7.9], S3( $n = 57$ ): min = 4.44; max = 17.6; whisker = [4.44–17.6]; median = [11.4], S4( $n = 72$ ): min = 13.32; max = 23.82; whisker = [13.32–23.82];

median = [19.3], S5( $n = 61$ ): min = 13.08; max = 27.97; whisker = [13.08–27.97]; median = [22.05], S6( $n = 57$ ): min = 18.89; max = 30.04; whisker = [18.89–30.04]; median = [22.92], S7( $n = 60$ ): min = 16.69; max = 32.53; whisker = [16.69–32.53]; median = [24.65]. **d**, Cell growth curve of YBX1 phosphomutants expressing Ba/F3 JAK2VF cells following treatment with increase doses of JAK inhibitor (1 nM–10  $\mu$ M RUX) measured by MTS assay.  $n = 4$  independent experiments each with 8 technical replicates. **e**, FACS plots showing induction of apoptosis in Ba/F3 JAK2VF cells expressing YBX1 phosphomutants following JAK inhibitor treatment (RUX, 0.5  $\mu$ M) compared to untreated YBX1 wild-type Ba/F3 JAK2VF cells. **f**, Bar plot shows quantification of the percentages of apoptotic (annexin V- and 7-AAD-positive) cells.  $n = 6$  independent experiments since YBX1 phosphomutants endogenously express GFP,  $n = 3$  for annexin V-APC staining and  $n = 3$  for 7-AAD-APC staining (error bars represent mean  $\pm$  s.d.).



Extended Data Fig. 7 | See next page for caption.

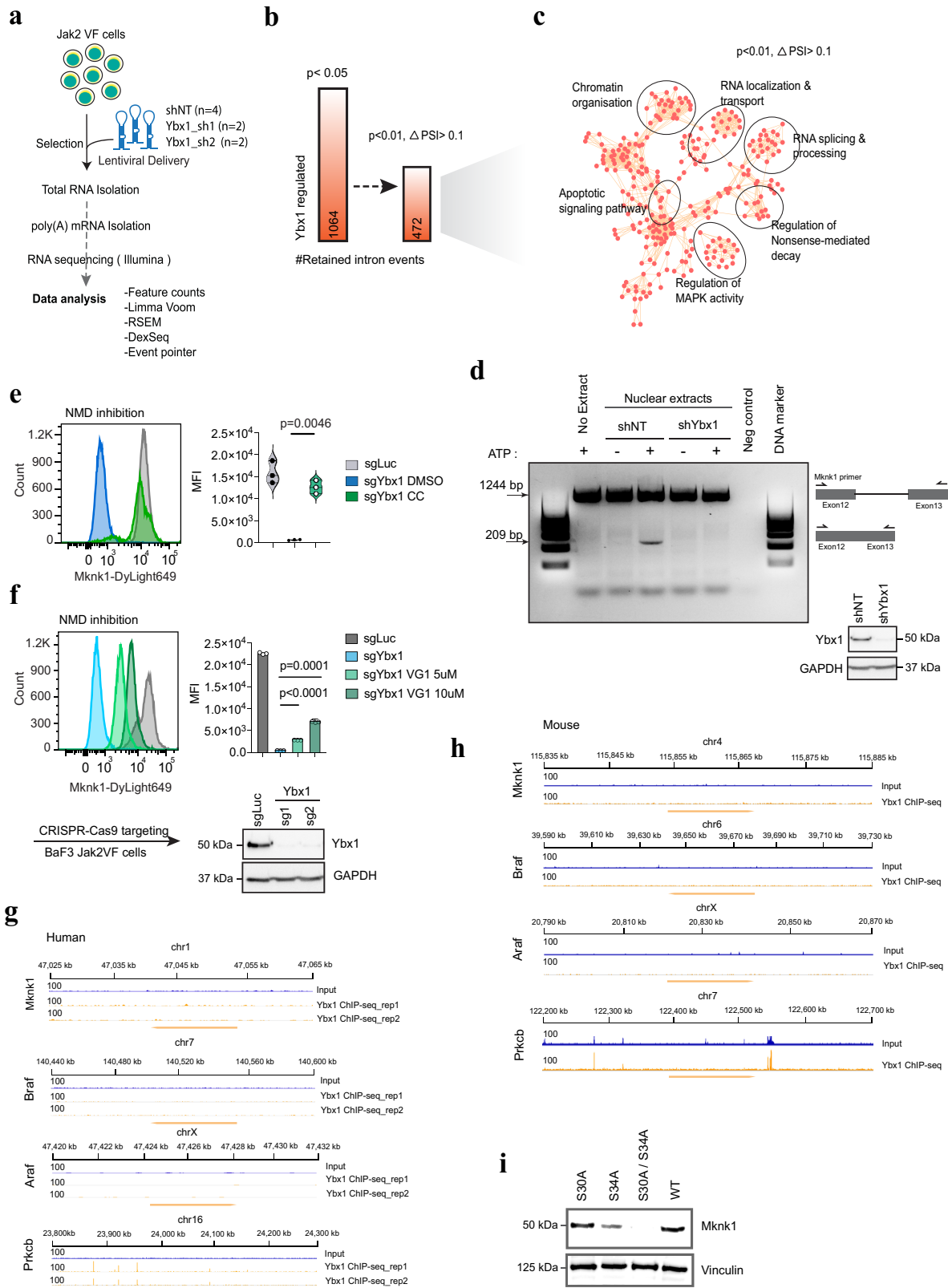


# Article

## Extended Data Fig. 7 | MEK-inhibition prevents YBX1 nuclear localization in *Jak2*-mutated cells. **a**, Confocal images of YBX1 localization (Red) in Ba/F3

JAK2VF cells after treatment for 2 h with RUX (0.5  $\mu$ M), MEK inhibitor (2  $\mu$ M), the ERK inhibitor trametinib (Tram; 100 and 200 nM), RUX + Tram or DMSO (control). Cells were counterstained with DAPI. **b**, Bar plot shows quantification of nuclear YBX1 expression in Ba/F3 JAK2VF cells ( $n \geq 3$  independent imaging experiments,  $P$  value determined by Student's  $t$ -test). DMSO ( $n = 67$ ): min = 7.05; max = 27.27; whisker = [7.05–27.27]; median = [15.01], RUX ( $n = 77$ ): min = 6.6; max = 35.8; whisker = [6.6–35.8]; median = [16.39], CGP57380 ( $n = 89$ ): min = 3.2; max = 16.35; whisker = [3.2–16.35]; median = [8.35], Tram ( $n = 67$ ): min = 2.44; max = 14.18; whisker = [2.44–14.18]; median = [12.01], Tram ( $n = 62$ ): min = 2.5; max = 17.96; whisker = [2.5–17.96]; median = [12.01], Tram + RUX ( $n = 64$ ): min = 3.44; max = 19.23; whisker = [3.44–19.23]; median = [13.04], MEK inhibitor + RUX ( $n = 68$ ): min = 4.06; max = 14.68; whisker = [4.06–14.68]; median = [13.01]. **c**, Bubble plot showing the regulation of human YBX1 pS32 and pS36 phosphorylation in HEL cells treated with RUX (0.5  $\mu$ M), CGP57380 (10  $\mu$ M), Tram (500 nM and 2  $\mu$ M) or DMSO (control) for 4 h in vitro. Phosphorylation

status of MAPK and JAK2 is shown as successful inhibition of respective targets of the corresponding kinase inhibitors.  $n = 4$  biological samples per group. Size and colour of bubbles are proportional to the z-scored log<sub>2</sub> phosphosite intensity; significance assessed using multiple sample test. **d**, Confocal images of YBX1 localization (red) in HEL cells treated with inhibitors or DMSO for 2 h. Cells were counterstained with DAPI.  $n = 3$  biological experiments. **e**, Bar plot shows quantification of nuclear YBX1 expression in HEL cells;  $P$  values were determined by Student's  $t$ -test. DMSO ( $n = 44$ ): min = 17.51; max = 34.56; whisker = [17.51–34.56]; median = [24.30], RUX ( $n = 44$ ): min = 13.04; max = 36.92; whisker = [13.04–36.92]; median = [23.9], MEK inhibitor ( $n = 41$ ): min = 7.62; max = 15.36; whisker = [7.62–15.36]; median = [11.89], Tram ( $n = 48$ ): min = 6.38; max = 19.03; whisker = [6.38–19.03]; median = [12.01], Tram + RUX ( $n = 55$ ): min = 3.31; max = 19.19; whisker = [3.31–19.19]; median = [13.04], MEK inhibitor + RUX ( $n = 49$ ): min = 4.32; max = 19.46; whisker = [4.32–19.46]; median = [13.01]. **f**, Immunoprecipitation of YBX1 from Ba/F3 JAK2VF cells expressing YBX1 phosphomutants.  $n = 3$  independent experiments.

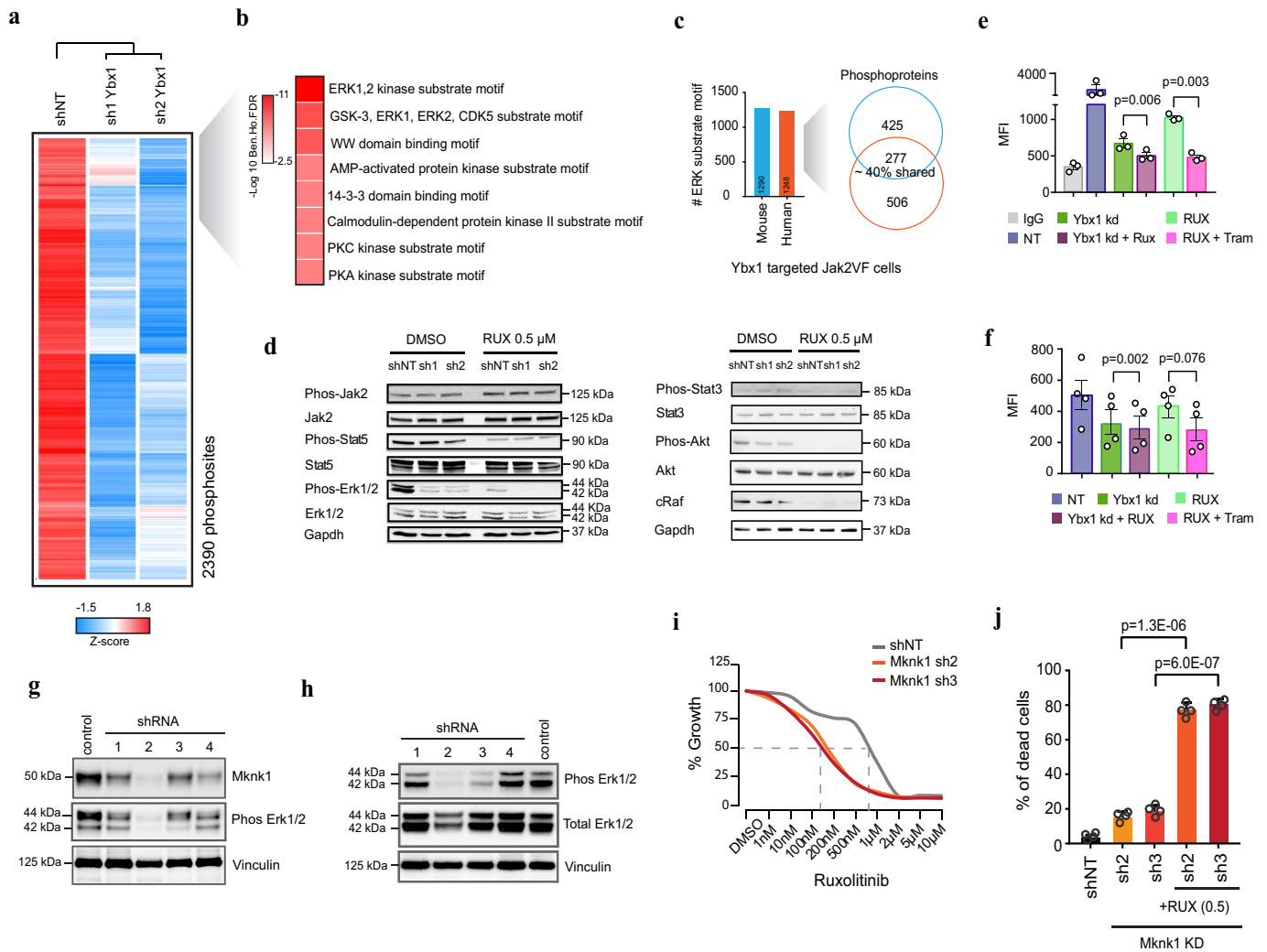


Extended Data Fig. 8 | See next page for caption.

# Article

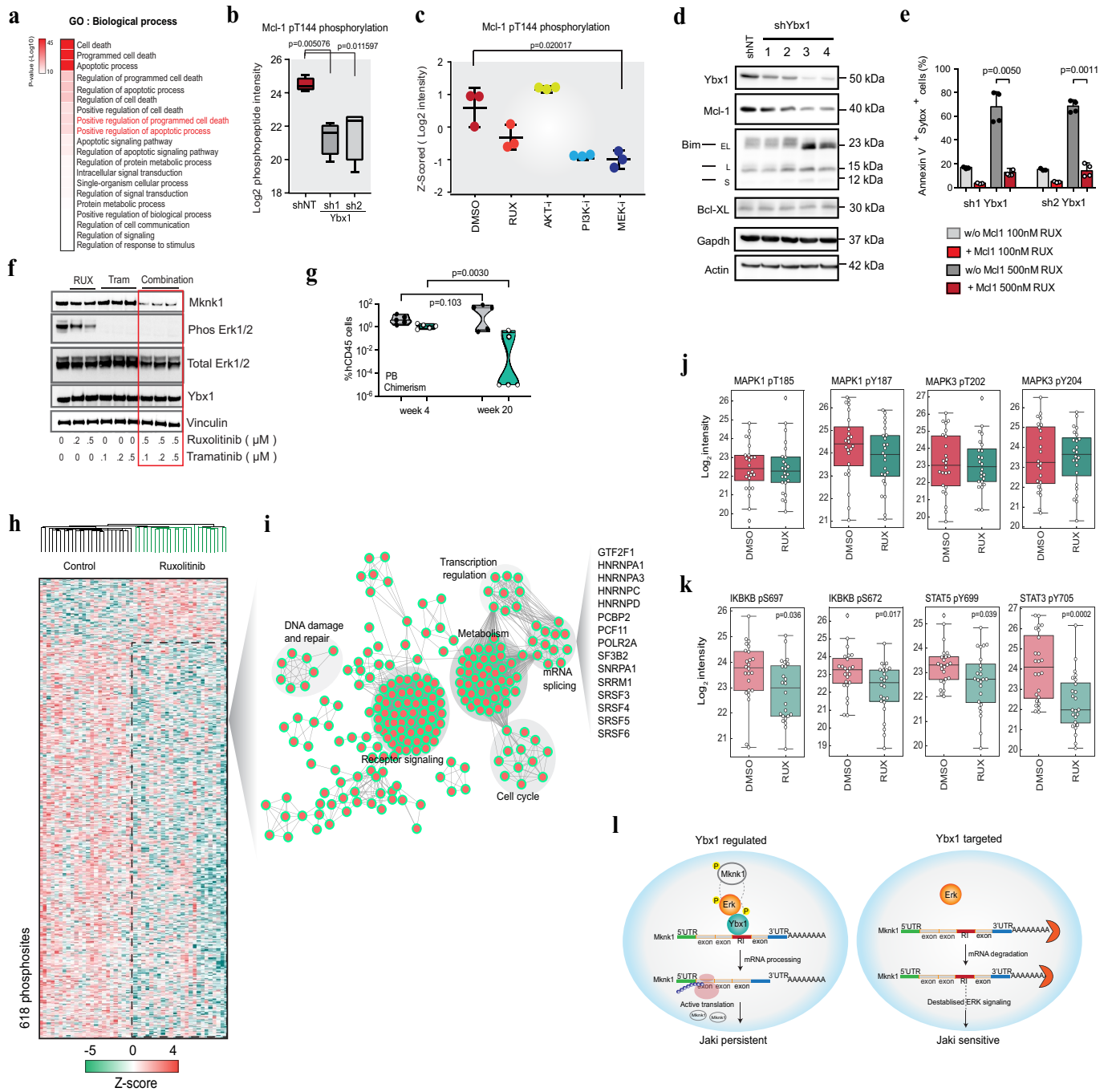
**Extended Data Fig. 8 | Nuclear YBX1 regulates *Mknk1* mRNA splicing in JAK2VF cells.** **a**, Experimental design of RNA sequencing and data analysis. **b**, Bars represent number of retained intron events significantly upregulated in YBX1-depleted cells with two-tailed test  $P$  value  $< 0.05$  (1,064 RI events), then filtered for  $P$  value  $< 0.01$  and  $\Delta$ PSI 0.1, reducing the number to 472 highly significant RI events. **c**, Network map displaying enrichment of gene sets in the 472 highly significant RI events. Each node represents significantly enriched gene sets. Clusters of functionally related gene sets are circled, and labels are highlighted. Two-sided hypergeometric test,  $P$  value correction–Bonferroni step down. **d**, Visualization of spliced *Mknk1* mRNA product after in vitro splicing assay. Nuclear extracts with and without YBX1 knockdown and with and without ATP were incubated for 2 h with biotin-labelled *Mknk1* pre-mRNA (exon 12–exon 13). mRNA was isolated and reverse transcribed, PCR was performed using the primers at the indicated arrow, and products were agarose gel resolved and visualized using gel-red stain. Representative images

from  $n = 3$  biological experiments. **e, f**, Flow cytometric analysis of MKNK1 protein expression rescue experiment in CRISPR–Cas9-induced YBX1 knockout mouse JAK2VF cells upon nonsense-mediated decay (NMD) inhibition. Representative flow cytometry histogram and violin plot showing quantification of MKNK1–DyLight 649 mean fluorescence intensity (MFI) upon **e**, compound C treatment (NMD inhibitor (dorsomorphin), termed CC, 10  $\mu$ M, for 24 h), and **f**, VG-1 treatment (5  $\mu$ M and 10  $\mu$ M, for 20 h) ( $n = 3$ , two-sided  $t$ -test; mean  $\pm$  s.d.). **g**, Genomic track profile of human *MKNK1*, *ARAF* and *BRAF* loci in HEL cells from YBX1 ChIP sequence data set ( $n = 2$ ). **h**, Genomic track profile of mouse *Mknk1*, *Araf* and *Braf* loci in Ba/F3 JAK2VF cells from YBX1 ChIP sequence data set.  $n = 3$  biological experiments. Genomic track profile of human and mouse *Prkcb* shown as positive control from the YBX1 ChIP-seq data set compared to IgG controls. **i**, Western blot showing the regulation of MKNK1 protein abundance in YBX1 phosphomutants expressing Ba/F3 JAK2VF cells as indicated.  $n = 3$  independent experiments.



**Extended Data Fig. 9 | Targeting *Mknk1* deregulates ERK signalling in *Jak2*-mutated cells.** **a**, Unsupervised hierarchical clustering of significantly down regulated phosphosites ( $n = 2,390$  sites) in human HEL cells following inactivation of *YBX1* by two independent shRNAs compared to non-targeting control.  $n = 4$  biological replicates. Heatmap represents z-scored and averaged log<sub>2</sub> phosphosite intensity, significance by ANOVA test with permutation-based FDR < 0.01. **b**, Kinase-substrate motifs significantly downregulated in *YBX1*-targeted HEL cells are shown including Benjamini-Hochberg FDR value ( $-\log_{10}$ ). **c**, ERK substrate motifs significantly downregulated and shared between *Ybx1*-targeted mouse and human JAK2VF cells. **d**, Western blot analysis of total protein abundance and phosphorylation of JAK2 downstream targets upon treatment with JAK inhibitor and/or genetic inactivation of *YBX1* by RNAi. GAPDH used as loading control. Representative images from  $n = 3$  independent experiments. **e**, **f**, Bar plots show the mean fluorescence intensity of pERK levels measured in human HEL (**e**;  $n = 3$ ) and in

patient *JAK2*-mutated cells (**f**;  $n = 4$  independent biological replicates from 4 individual patients) following genetic inactivation of *YBX1* by RNAi with or without drug treatment as indicated. Representative FACS plots shown in Fig. 4d. Data shown as mean  $\pm$  s.d. and  $P$  value determined by two-tailed Student's  $t$ -test. **g**, Western blot validation of *Mknk1*-targeting shRNAs in mouse Ba/F3 JAK2VF cells. **h**, Representative western blot analysis of pERK upon genetic inactivation of *Mknk1* in Ba/F3 JAK2VF cells.  $n = 4$  with comparable results. **i**, Growth curve of JAK2VF cells following lentiviral infection with shRNAs targeting *Mknk1* or non-targeting control and treatment with increase doses of JAK inhibitor (1nM–10 μM RUX) measured by MTS assay.  $n = 4$ , each with 8 technical replicates. **j**, Percentage of apoptotic JAK2VF cells following lentiviral knockdown of *Mknk1* (sh2, sh3  $\pm$  RUX 0.5 μM) or infection with non-targeting control (shSCR) ( $n = 4$ , two-tailed Student  $t$ -test, mean  $\pm$  s.d.).



Extended Data Fig. 10 | See next page for caption.

**Extended Data Fig. 10 | MCL-1 rescue of *Ybx1*-targeted cells and phosphoproteome analysis of primary *Jak2*-mutated cells upon JAK inhibitor treatment.** **a**, Proteome analysis of mouse *Jak2*-mutated cells following inactivation of *Ybx1* by two shRNAs compared to non-targeting control. Heatmap representation of significantly enriched GO term biological processes in YBX1-depleted JAK2VF cells assessed by Fisher's exact test ( $P(-\log_{10})$  shown). **b**, Quantification of MCL-1 phosphosite pT144 in sh1Ybx1, sh2Ybx1 and shNT control in mouse JAK2VF cells. The y axis is the  $\log_2$  intensity of the phosphopeptide ( $n = 4$  biological replicates, two-tailed Student *t*-test). shNT: min = 23.8; max = 24.7; whisker = [23.8–24.7]; box = [24–24.2], sh1Ybx1: min = 19.8; max = 22; whisker = [19.8–22]; box = [21.3–21.6], sh2Ybx1: min = 19.2; max = 22.4; whisker = [19.2–22.4]; box = [21.8–22.4]. **c**, Scatter dot plot of MCL-1 phosphosite pT144 after respective kinase inhibitor treatment ( $n = 3$ , biological replicates, *P* values using two-tailed Student *t*-test, error bars represent  $\pm$  s.d.). The y axis is the z-scored,  $\log_2$  phosphopeptide intensity. DMSO: min = -0.09; whisker = [-0.09 to 1.02], RUX: min = -0.554; max = 0.135; whisker = [-0.55 to 0.135], AKT inhibitor: min = 1.071; max = 1.263; whisker = [1.07–1.2634], PI3Ki: min = -1.008; max = -0.89; whisker = [-1.008 to 0.89], MEK inhibitor: min = -1.266; max = -0.699; whisker = [-1.266 to 0.699]. **d**, Western blot analysis of MCL-1, YBX1, BIM and BCL-XL following genetic inactivation of *Ybx1* with four different shRNA constructs, compared to non-targeting control.  $n = 3$  independent experiments. **e**, Measurement of apoptosis (annexin V- and Sytox-positive cells) after genetic inactivation of *Ybx1* and concomitant JAK inhibitor treatment (RUX, 100 nM, 500 nM). Rescue by ectopic overexpression of MCL-1 ( $n = 4$  independent experiments, two-tailed *t*-test). **f**, Western blot analysis of Ba/F3 JAK2VF cells showing downregulation of MKNK1 protein abundance following overnight combination treatment with RUX and Tram.  $n = 3$  biological independent experiments. **g**, Peripheral blood cell analysis of human cell chimerism in NSGW41 humanized mice at week 4 and 20 ( $n = 5$  per cohort). **h**, Heatmap shows unsupervised hierarchical clustering of significantly regulated (*t*-test with permutation-based FDR < 0.01) phosphosites with ( $n = 24$ ) and without ( $n = 24$ ) JAK inhibitor treatment in

*Jak2*-mutated primary patient samples. Phosphoproteome analysis of *Jak2*-mutated primary patient samples (total  $n = 48$ ) samples following in vitro ( $n = 18$ , JAK inhibitor treatment for 2 h) or in vivo ( $n = 6$ , 2 h post dosing of RUX samples) exposure to ruxolitinib. **i**, Network map of significantly enriched GO terms ( $P$  value < 0.01) of dephosphorylated proteins upon JAK inhibitor treatment. Two-sided hypergeometric test, *P* value correction–Bonferroni step down. **j**, Box plot shows no significant changes in the MAPK1 and MAPK3 phosphorylation in control ( $n = 24$ ) vs JAK inhibitor treated ( $n = 24$ ) patient samples. MAPK1pT185 (DMSO): min = 19.61; max = 24.82; whisker = [19.61–24.82]; box = [21.34–23.11], MAPK1pT185 (RUX): min = 19.5; max = 24.81; whisker = [19.5–24.81]; box = [21.64–23.72], MAPK1pY187 (DMSO): min = 21.04; max = 26.45; whisker = [21.04–26.45]; box = [23.22–25.46], MAPK1pY187 (RUX): min = 21.09; max = 25.89; whisker = [21.09–25.89]; box = [22.63–24.77], MAPK3pT202 (DMSO): min = 19.72; max = 26.06; whisker = [19.72–26.06]; box = [21.46–24.78], MAPK3pT202 (RUX): min = 20.41; max = 26.93; whisker = [20.41–26.93]; box = [22.05–23.88], MAPK3pY204 (DMSO): min = 20.70; max = 26.51; whisker = [20.70–26.51]; box = [22.02–24.99], MAPK3pY204 (RUX): min = 20.31; max = 25.76; whisker = [20.31–25.76]; box = [22.72–24.42]. **k**, Box plot shows significant changes in IKKKB, STAT3 and STAT5 phosphorylation in control ( $n = 24$ ) vs JAK inhibitor treated ( $n = 24$ ) patient samples. *P* values as determined by Mann–Whitney test. IKKKBpS697 (DMSO): min = 20.66; max = 25.79; whisker = [20.66–25.79]; box = [22.89–24.40], IKKKBpS697 (RUX): min = 20.66; max = 25.04; whisker = [20.66–25.04]; box = [21.88–23.88], IKKKBpS672 (DMSO): min = 20.71; max = 26.30; whisker = [20.71–26.30]; box = [22.5–23.86], IKKKBpS672 (RUX): min = 18.85; max = 24.73; whisker = [18.85–24.73]; box = [21.44–23.24], STAT5pY699 (DMSO): min = 22.02; max = 25.33; whisker = [22.02–25.33]; box = [22.73–23.63], STAT5pY699 (RUX): min = 19.90; max = 24.83; whisker = [19.90–24.83]; box = [21.8–23.2], STAT3pY705 (DMSO): min = 21.87; max = 26.66; whisker = [21.87–26.66]; box = [22.41–25.62], STAT3pY705 (RUX): min = 20.07; max = 26.17; whisker = [20.07–26.17]; box = [21.22–23.26]. **l**, Schematic depicting the mechanism of YBX1-mediated JAK inhibitor persistence.



## Reporting Summary

Nature Research wishes to improve the reproducibility of the work that we publish. This form provides structure for consistency and transparency in reporting. For further information on Nature Research policies, see [Authors & Referees](#) and the [Editorial Policy Checklist](#).

### Statistics

For all statistical analyses, confirm that the following items are present in the figure legend, table legend, main text, or Methods section.

n/a Confirmed

- The exact sample size ( $n$ ) for each experimental group/condition, given as a discrete number and unit of measurement
- A statement on whether measurements were taken from distinct samples or whether the same sample was measured repeatedly
- The statistical test(s) used AND whether they are one- or two-sided  
*Only common tests should be described solely by name; describe more complex techniques in the Methods section.*
- A description of all covariates tested
- A description of any assumptions or corrections, such as tests of normality and adjustment for multiple comparisons
- A full description of the statistical parameters including central tendency (e.g. means) or other basic estimates (e.g. regression coefficient) AND variation (e.g. standard deviation) or associated estimates of uncertainty (e.g. confidence intervals)
- For null hypothesis testing, the test statistic (e.g.  $F$ ,  $t$ ,  $r$ ) with confidence intervals, effect sizes, degrees of freedom and  $P$  value noted  
*Give  $P$  values as exact values whenever suitable.*
- For Bayesian analysis, information on the choice of priors and Markov chain Monte Carlo settings
- For hierarchical and complex designs, identification of the appropriate level for tests and full reporting of outcomes
- Estimates of effect sizes (e.g. Cohen's  $d$ , Pearson's  $r$ ), indicating how they were calculated

*Our web collection on [statistics for biologists](#) contains articles on many of the points above.*

### Software and code

Policy information about [availability of computer code](#)

#### Data collection

Flow cytometry data was acquired using the FACSDiva software, version 8.0.3; for detection of protein signals by Western blot, the GeneSys software, version 1.5.7.0 was used; measurement of murine blood was performed using the BC-5000 software; LC-MS/MS measurement: X-caliber software, version 4.0.27.19 (Thermo Fisher Scientific, Waltham, MA, USA);

#### Data analysis

For Phosphoproteome, Proteome and Interactome data analysis, Maxquant, version 1.5.5.2 (<https://www.nature.com/articles/nprot.2016.136>) and Perseus, version 1.5.2.11 (<https://www.nature.com/articles/nmeth.3901>) was used. Enrichment analysis was performed with ClueGO app in the Cytoscape, version 3.5.1 and for interaction networks string database applied. The dot plot presented in Extended Figure\_6 was made using a simple R script, it is available on request.

For RNA Sequencing, the reads were filtered, trimmed and then mapped to the Ensembl gene annotation and the mouse genome assembly GRCh38 using STAR aligner (Dobin, A. et al) with ENCODE settings in two-pass mode considering splice junctions across all samples in the second mapping step. Gene counts were quantified using featureCounts (Liao, Y et al) and differential expression calculated with the limma-voom pipeline (Ritchie, M. E. et al). Gene and transcript expression levels were quantified using RSEM. Event level differential splicing was calculated with the EventPointer package (Ritchie, M. E. et al) in R.

For ChIP seq data the reads were filtered, trimmed (FASTX-Toolkit, version 0.0.14; TrimGalore, version 0.4.4), mapped (using segemehl, version 0.2.0-418) and aligned the reads to hg19 genome for human and GRCh38 genome for mouse using Bowtie2, version 2.4.0. MACS2, version 2.1.1 was used to call peaks at q-value assigned to 0.01. HOMER, version 4.11 was used to call motifs. Analysis was performed using "basepair", version 3 (basepairtech.com) utilizing the default settings.

Analysis of flow cytometry data was performed using FlowJoTM software, version 8.8.6 (Treestar, Ashland, OR).

Western blot, immunohistochemistry and immunofluorescence images were analysed using ImageJ software, version 1.47v; Java 1.6.0\_65 (<http://rsb.info.nih.gov>).

For survival analysis, Kaplan-Meier curves were plotted using GraphPad Prism TM, version 6.0h (GraphPad Software, San Diego, CA, USA).

The dot plot presented in Extended Figure\_6 made using a simple R script as below  

```
bubbledata = read.table("bubbleplot_datamatrix.txt", sep = "\t", header = TRUE)
bubbledata$NewCol <- paste( bubbledata$Amino.acid, bubbledata$Position, sep="")
```

```
bubbledata$NewColname <- paste(bubbledata$Gene.names, bubbledata$NewCol, sep='')
newdf=bubbledata[1:8]
newdff = cbind(newdf,bubbledata$NewColname)
newmat = melt(newdff)
names(newmat) = c('genename', 'some', 'frequency')
ggplot(newmat, aes(x =some, y = genename, size = frequency, color = frequency)) + geom_point()+ scale_size_continuous(range = c(0, 5))+scale_color_gradient2(low="blue",mid="cyan", high = "red").
```

For manuscripts utilizing custom algorithms or software that are central to the research but not yet described in published literature, software must be made available to editors/reviewers. We strongly encourage code deposition in a community repository (e.g. GitHub). See the Nature Research [guidelines for submitting code & software](#) for further information.

## Data

Policy information about [availability of data](#)

All manuscripts must include a [data availability statement](#). This statement should provide the following information, where applicable:

- Accession codes, unique identifiers, or web links for publicly available datasets
- A list of figures that have associated raw data
- A description of any restrictions on data availability

The MS raw data files and Maxquant output files reported in this manuscript are available at ProteomeXchange Consortium with the data identifier PXD006921. RNA-seq data have been deposited in the Gene expression Omnibus database with accession number GSE123417. ChIP-seq data has been deposited to the Gene expression Omnibus database with the accession code GSE154025 for mouse and GSE146717 for human.

## Field-specific reporting

Please select the one below that is the best fit for your research. If you are not sure, read the appropriate sections before making your selection.

- Life sciences       Behavioural & social sciences       Ecological, evolutionary & environmental sciences

For a reference copy of the document with all sections, see [nature.com/documents/nr-reporting-summary-flat.pdf](https://www.nature.com/documents/nr-reporting-summary-flat.pdf)

## Life sciences study design

All studies must disclose on these points even when the disclosure is negative.

Sample size

Proteome, Phosphoproteome, Interactome, RNA seq, ChIP Seq sample sizes were determined based on the authors' experience of what is necessary to generate a convincing and compelling result. Effect sizes in the experiments are such that any reasonable observer would conclude that the sample sizes employed in the manuscript are sufficient to support the conclusions. For all other experiments, no statistical method was used to predetermine sample size. For each experiment the n values are reported in the respective figure legend. We used standard sample sizes (please see below in "Replication") based on previous experiments and literature which are needed to perform an appropriate statistical test.

Data exclusions

No data was excluded for any reasons.

Replication

All the samples in this study were collected as biological replicates and data are highly reproducible. Except the proteome, phosphoproteome, Interactome, RNA sequencing, ChIP sequencing (biological replicates were used here for measurements), every experiment was performed several times with essentially the same result. Cell growth assays, apoptosis measurements, intracellular flow cytometry and colony-forming unit assays were performed as 3-5 independent experiments (exact number is mentioned in the respective figure legend). Western blots were done as 3 independent experiments. All mouse experiments were performed with 2-3 independent cohorts per experiment.

Randomization

In pre-clinical patient-derived xenograft mouse models paired-samples of patient cells were investigated for response to drug-treatment versus diluent control. Therefore, no randomization was necessary. Likewise, murine cells that were either genetically modified or pharmacologically treated were injected at equal distribution into recipient mice. Patient samples have been investigated for protein expression in an unbiased manner and were only selected for the relevant MPN driver mutation (JAK2V617F). Treatment intervention was performed in paired samples, therefore no randomization was necessary.

Blinding

Due to the analysis in paired samples, with pharmacologic therapy or diluent control, no blinding was necessary and possible at the stage of cell transplantation or drug treatment. For flow cytometry analysis of murine bone marrow (and xenograft) samples, the scientist analyzing the cell samples was blinded in regard to engrafted sample and treatment intervention.

## Reporting for specific materials, systems and methods

We require information from authors about some types of materials, experimental systems and methods used in many studies. Here, indicate whether each material, system or method listed is relevant to your study. If you are not sure if a list item applies to your research, read the appropriate section before selecting a response.

## Materials &amp; experimental systems

## Methods

n/a	Included in the study
<input type="checkbox"/>	<input checked="" type="checkbox"/> Antibodies
<input type="checkbox"/>	<input checked="" type="checkbox"/> Eukaryotic cell lines
<input checked="" type="checkbox"/>	<input type="checkbox"/> Palaeontology
<input type="checkbox"/>	<input checked="" type="checkbox"/> Animals and other organisms
<input type="checkbox"/>	<input checked="" type="checkbox"/> Human research participants
<input checked="" type="checkbox"/>	<input type="checkbox"/> Clinical data

n/a	Included in the study
<input type="checkbox"/>	<input checked="" type="checkbox"/> ChIP-seq
<input type="checkbox"/>	<input checked="" type="checkbox"/> Flow cytometry
<input checked="" type="checkbox"/>	<input type="checkbox"/> MRI-based neuroimaging

## Antibodies

## Antibodies used

The following antibodies were purchased from Cell Signaling (Danvers, MA, USA) and used at a 1: 1000 dilution: GFP (#2555; Lot#6), Mknk1 (#2195; Lot#5), p-Akt (#9271; Lot#14), Akt (#9272; Lot#25), p-p44/42 MAPK (#9106; Lot#45), p44/42 MAPK (#9102; Lot#26 and #4695; Lot#21), cRaf (#9422; Lot#8), p-JAK2 (#3771; Lot#10), JAK2 (#3230; Lot#8), pSTAT3 (#9134; Lot#12), STAT3 (#9139; Lot#10), Bim (#2933; Lot#6), and Bcl-XL (#2764; Lot#6). GAPDH antibody (#H86504M; Lot#22D12014; clone: B2534M; dilution 1: 5000) was purchased from Meridian Life Sciences (Memphis, TN, USA), p-Stat5 antibody (#05-495; Lot#3012064; clone: 8-5-2; dilution 1: 1000) was purchased from Millipore (Darmstadt, Germany) and Stat5 (#sc-1081; Lot#F1915; dilution 1: 100) antibody was purchased from Santa Cruz Biotechnologies (Dallas, TX, USA). Mcl-1 antibody (#600-401-394; Lot#28725; dilution 1:1000) was delivered by Rockland Immunochemicals (Limerick, PA, USA), Vinculin purchased from Sigma (#V9131; Lot#018M4779V dilution: 1: 5000), Pcbp1 (#ab168378; Lot#GR121943-8; dilution 1:1000) and Ybx1 antibody (#ab76149; Lot#GR221265-23; dilution 1:1000) was delivered by Abcam (Cambridge, UK).

For FACS analysis, biotinylated antibodies against Gr-1 (#108404; Lot#B236916; clone: RB6-8C5), B220 (#103204; Lot#B241118; clone: RA3-6B2), CD19 (#115504; Lot#B250292; clone: 6D5), CD3 (#100304; Lot#B276683; clone: 145-2C11), CD4 (#100404; Lot#B191781; clone: GK1.5), CD8 (#100704; Lot#B205917; clone: 53-6.7), TER119 (#116204; Lot#B272730; clone: TER-119) and IL7Ra (#121104; Lot#B176924; clone: SB/199) (all Biolegend, San Diego, CA, USA) were used in a 1:500 dilution for lineage staining. For surface staining of respective markers, the following antibodies (all purchased from Biolegend, San Diego, CA, USA) were used at a 1:100 dilution: CD45.1-PE (#110708; Lot#B233347; clone: A20), CD45.2-APC (#109814; Lot#B293270; clone: 104), CD150-PerCP/Cy5.5 (#115921; Lot#B220584; clone: TC15-12F12.2), Sca-1-PE (#108107; Lot#B249342; clone: D7), cKit-APC (#105818; Lot#B220273; clone: 2B8), Streptavidin-BV421 (#405226; Lot#B263940; clone: N/A), CD48-APC/Cy7 (#103431; Lot#B255055; clone: HM48-1), FcγR-PE/Cy7 (#101318; Lot#B288450; clone: 93), Gr1-Pacific Blue (#108430; Lot#B260631; clone: RB6-8C5), TER119-PE (#116207; Lot#B246093; clone: TER-119), CD19-PE/Cy7 (#115519; Lot#B259557; clone: 6D5), CD3-APC/Cy7 (#100222; Lot#B217176; clone: 17A2), Streptavidin-PerCP/Cy5.5 (#405213; Lot#B155387; clone: N/A), Sca-2-PE/Cy7 (#108114; Lot#B185136; clone: D7), cKit-APC/Cy7 (#105825; Lot#B254318; clone: 2B8), human CD45-AF647 (#304018; Lot#B202879; clone: HI30), CD34-FITC (#553733; Lot#5079527; clone: RAM34) was purchased from Becton Dickinson, Franklin Lakes, NY, USA).

For apoptosis measurement Annexin V-APC (#640912; Lot#B263821; clone: N/A; dilution: 1:50; purchased from Biolegend) was used.

For intracellular flow analysis the following antibodies were used: MNK1 (#711542; Lot#SC248688; clone: 6HCLC; dilution 1:100; Thermo Fisher Scientific, Waltham, MA, USA), DyLight 649 (#406406; Lot#B296939; clone: Poly 4064; dilution 1:100; Biolegend), p-p44/42 (ERK1/2) Alexa Fluor 647 (#131485; Lot#8; clone: 197G2; dilution 1:50; Cell Signaling).

Immunofluorescent staining was performed using the following antibodies: yH2AX pS139 (#2577; Lot#8; dilution 1:800; Cell Signaling), Ybx1 (#ab76149; Lot#GR221265-23; dilution 1:250; Abcam), donkey anti-rabbit antibody Alexa Fluor 488 (#A21206; dilution 1:200; Life Technologies), donkey anti-rabbit antibody Alexa Fluor 568 (#A11036; dilution 1:200; Life Technologies), JAK2-Cy3(#bs-0908R-Cy3; dilution 1:50; BLOSS, Woburn, MA, USA).

## Validation

<https://www.cellsignal.de/products/primary-antibodies/gfp-antibody/2555>; [https://www.cellsignal.de/products/primary-antibodies/mnk1-c4c1-rabbit-mab/2195?\\_=1598088986493&Ntt=2195&tahead=true](https://www.cellsignal.de/products/primary-antibodies/mnk1-c4c1-rabbit-mab/2195?_=1598088986493&Ntt=2195&tahead=true); <https://www.cellsignal.de/products/primary-antibodies/phospho-akt-ser473-antibody/9271>; <https://www.cellsignal.de/products/primary-antibodies/gfp-antibody/2555>; <https://www.sigmaaldrich.com/catalog/product/sigma/sab4200080>; <https://www.abcam.com/pcbp1-antibody-epr11055-ab168378.html>; <https://www.cellsignal.de/products/primary-antibodies/akt-antibody/9272>; <https://www.cellsignal.de/products/primary-antibodies/phospho-p44-42-mapk-erk1-2-thr202-tyr204-e10-mouse-mab/9106>; <https://www.cellsignal.de/products/primary-antibodies/p44-42-mapk-erk1-2-antibody/9102>; <https://www.cellsignal.de/products/primary-antibodies/c-raf-antibody/9422>; <https://www.cellsignal.de/products/primary-antibodies/phospho-jak2-tyr1007-1008-antibody/3771>; <https://www.cellsignal.de/products/primary-antibodies/jak2-d2e12-xp-rabbit-mab/3230>; <https://www.cellsignal.de/products/primary-antibodies/phospho-stat3-ser727-antibody/9134>; <https://www.cellsignal.de/products/primary-antibodies/stat3-124h6-mouse-mab/9139>; <https://www.cellsignal.de/products/primary-antibodies/bcl-xl-54h6-rabbit-mab/2764>; <https://www.cellsignal.de/products/primary-antibodies/bim-c34c5-rabbit-mab/2933>; <https://www.cellsignal.de/products/primary-antibodies/phospho-histone-h2a-x-ser139-antibody/2577>; <https://www.biomol.com/products/antibodies/primary-antibodies/general/anti-mcl-1-myeloid-cell-leukemia-1-600-401-394>; <https://meridianlifescience.com/bioSpecs/H86504M.pdf>; [https://www.merckmillipore.com/DE/de/product/Anti-phospho-STAT5A-B-Tyr694-699-Antibody-clone-8-5-2,MM\\_NF-05-495](https://www.merckmillipore.com/DE/de/product/Anti-phospho-STAT5A-B-Tyr694-699-Antibody-clone-8-5-2,MM_NF-05-495); <https://www.scbt.com/p/stat5a-antibody-l-20?requestFrom=search>; <https://www.sigmaaldrich.com/catalog/product/sigma/v9131?lang=de&region=DE>; <https://www.abcam.com/yb1-antibody-epr2708y-ab76149.html>; <https://www.abcam.com/pcbp1-antibody-epr11055-ab168378.html>; <https://www.thermofisher.com/antibody/product/MNK1-Antibody-clone-6HCLC-Recombinant-Polyclonal/711542>; <https://www.cellsignal.de/products/antibody-conjugates/phospho-p44-42-mapk-erk1-2-thr202-tyr204-197g2-rabbit-mab-alex-fluor-647-conjugate/13148>; <https://www.biolegend.com/de-de/products/alex-fluor-647-anti-human-cd45-antibody-2739>; <https://www.biolegend.com/de-de/>

products/percp-cyanine5-5-anti-mouse-cd150-slam-antibody-4290; <https://www.biolegend.com/de-de/products/pe-anti-mouse-ly-6a-e-sca-1-antibody-228>; <https://www.biolegend.com/de-de/products/alexa-fluor-647-anti-mouse-cd117-c-kit-antibody-3132>; <https://www.biolegend.com/de-de/products/brilliant-violet-421-streptavidin-7297>; <https://www.biolegend.com/de-de/products/apc-cyanine7-anti-mouse-cd48-antibody-8054>; <https://www.biolegend.com/de-de/products/pe-cyanine7-anti-mouse-cd16-32-antibody-6355>; <https://www.biolegend.com/de-de/products/pacific-blue-anti-mouse-ly-6g-ly-6c-gr-1-antibody-4143>; <https://www.biolegend.com/de-de/products/pe-cyanine7-anti-mouse-cd19-antibody-1907>; <https://www.biolegend.com/de-de/products/apc-cyanine7-anti-mouse-cd3-antibody-6068>; <https://www.biolegend.com/de-de/products/percp-streptavidin-4211>; <https://www.biolegend.com/de-de/products/pe-cyanine7-anti-mouse-ly-6a-e-sca-1-antibody-3137>; <https://www.biolegend.com/de-de/products/apc-cyanine7-anti-mouse-cd117-c-kit-antibody-5905>; <https://www.biolegend.com/de-de/products/alexa-fluor-647-annexin-v-5276>

## Eukaryotic cell lines

Policy information about [cell lines](#)

Cell line source(s)	Murine Ba/F3 cells stably expressing Jak2WT and Jak2VF (previously published cell line model that was in house created); human SET-2 (#ACC 608), HEL 92.1.7 (#ACC 11) and HEK293T (#ACC 305) cells were all purchased from DSMZ, Braunschweig, Germany.
Authentication	Cell lines were not authenticated.
Mycoplasma contamination	Cell lines were routinely tested and maintained mycoplasma free throughout the study. No cell lines were tested positive for mycoplasma.
Commonly misidentified lines (See <a href="#">ICLAC</a> register)	No commonly misidentified cell lines were used.

## Animals and other organisms

Policy information about [studies involving animals](#); [ARRIVE guidelines](#) recommended for reporting animal research

Laboratory animals	All animals were housed under pathogen-free conditions in the accredited Animal Research Facility at the Otto-von-Guericke University Magdeburg or the University Hospital Jena. Animals were maintained in groups in single-ventilated type II long IVC-cages. Room temperature was 22°C +/- 2°C and humidity was maintained at 55% +/- 10%. Mice were kept in rooms with light/dark cycle (6am-20pm: light; 20pm-6am: dark; including a twilight phase in between). Specification of sex and gender for the different mouse strains: Ybx1 +/- or Ybx1 -/- donor mice, females and males were used, age 6-8 week old; Ybx+/- VF_Mx or Ybx-/-_VF_Mx donor mice, females and males were used, age 6-8 week old; C57BL/6J (CD45.2) recipients, only females were used, age 6-8 week old; Ly5.1 (CD45.1) recipients, only females were used, age 6-8 week old; CD45.1/2 competitors, males and females were used (female competitors were paired with female donors and male competitors were paired with male donors), age 6-8 week old; NSGS recipients, only females were used, age 6-8 week old.
Wild animals	No wild animals were used in this study.
Field-collected samples	No field collected samples were used in this study.
Ethics oversight	All animal experiments have been approved by the respective ethics committees for animal welfare either at the Landesverwaltungsamt Saxony-Anhalt, Halle (State Administration Office Saxony-Anhalt) or at the Landesamt für Verbraucherschutz, Abteilung Gesundheitlicher und technischer Verbraucherschutz, Referat Verbraucherschutz und Veterinärangelegenheiten (Thuringian State Administration Office), Bad Langensalza, Thuringia, Germany.

Note that full information on the approval of the study protocol must also be provided in the manuscript.

## Human research participants

Policy information about [studies involving human research participants](#)

Population characteristics	Blood and bone marrow of patients with diagnosed classical chronic myeloproliferative neoplasms (MPN) according to the WHO 2008 or 2016 classifications and identification of JAK2V617F as the relevant driver mutation have been investigated in this study. All types of patient samples and healthy donor controls derived during routine biopsies (peripheral blood, bone marrow aspirates and biopsies) and investigated in this study were obtained after informed consent and according to the Helsinki declaration from the Tumor Banks in Jena and Magdeburg, Germany. Scientific protocol, patient information and patient approval forms have been approved by the respective local ethics committees.
Recruitment	Patients were identified from all MPN patients treated in each institution after informed consent within the indicated protocols. Patients harboring JAK2 mutations were identified by molecular standard diagnostics required for classification of the MPN entity and for diagnosis according to WHO criteria. The type of driver mutation (JAK2V617F) may lead to inclusion of more patients with polycythemia vera (PV) as the driver mutation is more prevalent in this disease subentity compared to essential thrombocythemia or myelofibrosis. Due to the inclusion of patients in a protocol at an academic institution (University Hospital), we cannot exclude a bias regarding patients with higher risk profiles compared to those not treated at academic institutions. However, this bias does may rather emphasize the validity of the results even in a higher-risk population.

Ethics oversight

'Ethics Committee, University Hospital Jena' #4753/04-16 and 'Ethics Committee, Medical Faculty, OvGU Magdeburg' #115/08

Note that full information on the approval of the study protocol must also be provided in the manuscript.

## ChIP-seq

### Data deposition

- Confirm that both raw and final processed data have been deposited in a public database such as [GEO](#).
- Confirm that you have deposited or provided access to graph files (e.g. BED files) for the called peaks.

Data access links

*May remain private before publication.*

Files uploaded to GEO with the accession number GSE154025 for the mouse and GSE146717 for human ChIPSeq data.

Files in database submission

HEL\_ChIP-input, HEL\_YBX1-ChIP\_rep1, HEL\_YBX1-ChIP\_rep2.  
BaF3JAK2VF\_Input1, BaF3JAK2VF\_Input2, and BaF3JAK2VF\_Input3.  
BaF3JAK2VF\_YBX1\_1, BaF3JAK2VF\_YBX1\_2, BaF3JAK2VF\_YBX1\_3.

Genome browser session

(e.g. [UCSC](#))For human: <http://tinyurl.com/ughey2e>  
For mouse : <https://genome.ucsc.edu/s/Ayeroslaviz/BaF3%2DJAK2VF>.

### Methodology

Replicates

YBX1-ChIPseq was performed in two biological replicates in HEL cells and biological triplicates in BaF3JAK2VF cells.

Sequencing depth

HEL\_YBX1-ChIP\_rep1: 20.989.185 reads (76.4% uniquely mapped); HEL\_YBX1-ChIP\_rep2: 25.026.360 reads (77.2% uniquely mapped); HEL\_input: 83.011.971 reads (79.2% uniquely mapped).  
read length: 37bp, paired end sequencing.  
BaF3\_JAK2VF\_YBX1\_1: 52.852.192 reads (70.6% uniquely mapped); BaF3\_JAK2VF\_YBX1\_2: 53.733.647 reads (70.5% uniquely mapped); BaF3\_JAK2VF\_YBX1\_3: 54.886.301 reads (70.4% uniquely mapped). BaF3JAK2VF\_Input1: 67.388.971 (60% uniquely mapped), BaF3JAK2VF\_Input2: 53.751.547 (60% uniquely mapped), and BaF3JAK2VF\_Input3: 49.308.963 (60% uniquely mapped). read length: 160bp, Single end sequencing.

Antibodies

anti-YB1, Abcam, EP2708Y, #ab76149

Peak calling parameters

after Alignment of reads to hg19 genome human and mus-musculus GRCm38 using Bowtie2, MACS2 was used to call peaks at q-value assigned to 0.01. HOMER was used to call motifs. Analysis was performed using "basepair" (basepairtech.com) utilizing the default settings for the respective pipelines for HEL\_input, HEL\_YBX1-ChIP\_rep1 and HEL\_YBX1-ChIP\_rep2, BaF3JAK2VF\_Input1, BaF3JAK2VF\_Input2, and BaF3JAK2VF\_Input3, BaF3JAK2VF\_YBX1\_1, BaF3JAK2VF\_YBX1\_2, BaF3JAK2VF\_YBX1\_3.

Data quality

Quality controls include FASTQC after demultiplexing of data, deduplication and adaptor trimming.  
HEL\_YBX1-ChIP\_rep1: 22874 total peaks called, 22869 of these peaks have a FDR<5% and enrichment >5 fold  
HEL\_YBX1-ChIP\_rep2: 17285 total peaks called, 17279 of these peaks have a FDR<5% and enrichment >5 fold  
BaF3JAK2VF\_YBX1\_1: 7053 total peaks called, FDR<1% and enrichment >1 fold  
BaF3JAK2VF\_YBX1\_2: 2678 total peaks called, FDR<1% and enrichment >1 fold  
BaF3JAK2VF\_YBX1\_3: 2827 total peaks called, FDR<1% and enrichment >1 fold

Software

the automated ChIPseq pipeline of [www.basepairtech.com](http://www.basepairtech.com) was used to perform the analysis. The IGV-viewer was utilized to visualize peaks at selected loci.

## Flow Cytometry

### Plots

Confirm that:

- The axis labels state the marker and fluorochrome used (e.g. CD4-FITC).
- The axis scales are clearly visible. Include numbers along axes only for bottom left plot of group (a 'group' is an analysis of identical markers).
- All plots are contour plots with outliers or pseudocolor plots.
- A numerical value for number of cells or percentage (with statistics) is provided.

### Methodology

Sample preparation

For immunophenotype analysis, peripheral blood cells, bone marrow or spleen cells were resuspended in PBS/1% FBS after erythrocyte lysis (PharmLyse™, BD Pharmingen). Unless otherwise stated, the following antibodies were used: Sorting and analysis of LSK-cells or Sca-1+cells were performed as previously described in Heidel, F.H et al, Cancer Stem Cells 2012 and J Exp Med 2012.

Instrument	Cells were sorted on a BD FACSAriaTM III, analysis of the cells was performed using a FACSCantoII™ (Becton-Dickinson) cytometer
Software	FlowJo™ software (Treestar, Ashland, OR, USA).
Cell population abundance	For analysis of murine bone marrow, at least 5x 10 <sup>5</sup> cells were recorded. For peripheral blood analysis, at least 1x 10 <sup>4</sup> cells were recorded following dead cell exclusion. For human Jak2V617F positive bone marrow samples, CD34 positive cells were sorted from bone marrow aspirates. Following culture and incubation with respective inhibitors, between 1.1x10 <sup>3</sup> and 12.7x10 <sup>4</sup> events (cells) could be recorded for analysis of apoptotic cells.
Gating strategy	Positive cell populations were defined by distinct negative cell populations within the same sample and/or isotype controls. Gating strategies for murine bone marrow and peripheral blood cells are provided in the Extended Data Figures/Supplementary Information.

Tick this box to confirm that a figure exemplifying the gating strategy is provided in the Supplementary Information.